

Generation of turbulence in Kelvin-Helmholtz vortices at the Earth's magnetopause: Magnetospheric Multiscale observations

Hiroshi Hasegawa^{1,1}, Takuma Nakamura^{2,2}, Daniel J Gershman^{3,3}, Yasuhiro Nariyuki^{4,4}, Viñas Adolfo^{3,3}, Barbara L. Giles^{3,3}, Benoit Lavraud^{5,5}, Christopher T. Russell^{6,6}, Yuri V. Khotyaintsev^{7,7}, Robert E Ergun^{8,8}, and Saito Yoshifumi^{9,9}

¹Institute of Space and Astronautical Science, JAXA

²Space Research Institute

³NASA Goddard Space Flight Center

⁴University of Toyama

⁵Institut de Recherche en Astrophysique et Planetologie - CNRS

⁶University of California Los Angeles

⁷Swedish Institute of Space Physics

⁸Univeristy of Colorado

⁹JAXA/ISAS

November 30, 2022

Abstract

The Kelvin-Helmholtz instability (KHI) at Earth's magnetopause and associated turbulence are suggested to play a role in the transport of mass and momentum from the solar wind into Earth's magnetosphere. We investigate electromagnetic turbulence observed in KH vortices encountered at the dusk flank magnetopause by the Magnetospheric Multiscale (MMS) spacecraft under northward interplanetary magnetic field (IMF) conditions in order to reveal its generation process, mode properties, and role. A comparison with another MMS event at the dayside magnetopause with reconnection but no KHI signatures under a similar IMF condition indicates that while high-latitude magnetopause reconnection excites a modest level of turbulence in the dayside low-latitude boundary layer, the KHI further amplifies the turbulence, leading to magnetic energy spectra with a power-law index $-5/3$ at magnetohydrodynamic scales even in its early nonlinear phase. The mode of the electromagnetic turbulence is analyzed with a single-spacecraft method based on Ampère's law, developed by Bellan (2016), for estimating wave vectors as a function of spacecraft-frame frequency. The results suggest that the turbulence does not consist of propagating normal-mode waves, but is due to interlaced magnetic flux tubes advected by plasma flows in the vortices. The turbulence at sub-ion scales in the early nonlinear phase of the KHI may not be the cause of the plasma transport across the magnetopause, but rather a consequence of three-dimensional vortex induced reconnection, the process that can cause an efficient transport by producing tangled reconnected field lines.

Generation of turbulence in Kelvin-Helmholtz vortices at the Earth's magnetopause: Magnetospheric Multiscale observations

H. Hasegawa¹, T. K. M. Nakamura², D. J. Gershman³, Y. Nariyuki⁴, A. F.-Viñas³, B. L. Giles³, B. Lavraud⁵, C. T. Russell⁶, Y. V. Khotyaintsev⁷, R. E. Ergun⁸, and Y. Saito¹

¹Institute of Space and Astronautical Science, Japan Aerospace Exploration Agency, Sagami-hara, Japan

²Space Research Institute, Austrian Academy of Sciences, Graz, Austria

³NASA Goddard Space Flight Center, Greenbelt, MD, USA

⁴Faculty of Human Development, University of Toyama, Toyama, Japan

⁵Institut de Recherche en Astrophysique et Planétologie, CNRS, UPS, CNES, Université de Toulouse, Toulouse, France

⁶Department of Earth, Planetary, and Space Sciences, University of California, Los Angeles, California, USA

⁷Swedish Institute of Space Physics, Uppsala, Sweden

⁸Department of Astrophysical and Planetary Sciences, University of Colorado, Boulder, Colorado, USA

Corresponding author: Hiroshi Hasegawa (hase@stp.isas.jaxa.jp)

Key Points:

- The Kelvin-Helmholtz instability amplifies electromagnetic fluctuations in the magnetopause boundary layer
- The turbulent fluctuations in the vortices may not be due to propagating waves but to magnetic structures, i.e., interlaced flux tubes
- The turbulence at sub-ion scales in an early nonlinear phase of the instability is likely a consequence of vortex induced reconnection

Abstract

The Kelvin-Helmholtz instability (KHI) at Earth's magnetopause and associated turbulence are suggested to play a role in the transport of mass and momentum from the solar wind into Earth's magnetosphere. We investigate electromagnetic turbulence observed in KH vortices encountered at the dusk flank magnetopause by the Magnetospheric Multiscale (MMS) spacecraft under northward interplanetary magnetic field (IMF) conditions in order to reveal its generation process, mode properties, and role. A comparison with another MMS event at the dayside magnetopause with reconnection but no KHI signatures under a similar IMF condition indicates that while high-latitude magnetopause reconnection excites a modest level of turbulence in the dayside low-latitude boundary layer, the KHI further amplifies the turbulence, leading to magnetic energy spectra with a power-law index $-5/3$ at magnetohydrodynamic scales even in its early nonlinear phase. The mode of the electromagnetic turbulence is analyzed with a single-spacecraft method based on Ampère's law, developed by Bellan (2016), for estimating wave vectors as a function of spacecraft-frame frequency. The results suggest that the turbulence does not consist of propagating normal-mode waves, but is due to interlaced magnetic flux tubes advected by plasma flows in the vortices. The turbulence at sub-ion scales in the early nonlinear phase of the KHI may not be the cause of the plasma transport across the magnetopause, but rather a consequence of three-dimensional vortex induced reconnection, the process that can cause an efficient transport by producing tangled reconnected field lines.

Plain Language Summary

Turbulence is ubiquitous in nature and plays an important role in material mixing and energy transport. Turbulence in space plasmas is characterized by fluctuations of flow velocity and/or electromagnetic fields over a broad frequency range and/or length scales, and is believed to be the key to efficient plasma transport and heating. However, its generation mechanism is not fully understood because turbulence in space is often fully developed or already relaxed when observed. By analyzing high-resolution plasma and electromagnetic field data taken by the Magnetospheric Multiscale spacecraft, we study the generation process of electromagnetic turbulence at the outer boundary of Earth's magnetosphere, called the magnetopause, where either a flow shear-driven Kelvin-Helmholtz instability or magnetic reconnection or both could drive turbulence. It is shown that while dayside reconnection generates a modest level of turbulence at the magnetopause near noon, the flow shear instability further amplifies the turbulence at the flank magnetopause. Our analysis also suggests that the turbulence may not be the primary cause of plasma transport from solar wind into the magnetosphere, but rather a consequence of the flow shear-induced reconnection that is likely the primary cause of plasma transport at the dayside flank under northward solar wind magnetic field conditions.

1 Introduction

Turbulence is ubiquitous in nature, such as in ocean (Smyth & Moum, 2012), planetary atmospheres (Wyngaard, 1992; Vasavada & Showman, 2005), solar/stellar convection zones (Miesch et al., 2000), accretion disks (Balbus & Hawley, 1998), and interstellar gas (Gaensler et al., 2011), and is believed to play a key role in material mixing and energy transfer in both configuration and wave number space. Turbulence in plasmas is characterized by broadband fluctuations of not only flows but also electromagnetic fields, and has been extensively and intensively studied in the solar wind community (e.g., Bruno & Carbone, 2013; Chen, 2016). While the turbulent cascade and dissipation processes at kinetic scales have been the focus of

recent studies on space plasma turbulence (Alexandrova et al., 2009, 2013; Narita, Nakamura, et al., 2016; Sahraoui et al., 2009; Phan et al., 2018), its generation mechanism is not fully understood; the turbulent energy injection process remains an open issue. This is partly because turbulence observed in the solar wind near 1 AU is often fully developed or may already be relaxed, leaving no or little information on how it is generated, although Parker Solar Probe (Fox et al., 2016), launched in 2018 and making in-situ measurements of the inner heliosphere and solar corona, is going to reveal the generation, or at least evolution, process of solar wind turbulence.

Plasma turbulence is common in the geospace environment as well (Zimbardo et al., 2010; Karimabadi et al., 2014). The geospace may be an ideal natural laboratory to study the generation of turbulence in a collisionless plasma, because various regions (bow shock, magnetopause, tail plasma sheet) or processes occurring there (magnetic reconnection, Kelvin-Helmholtz instability (KHI), wave-particle interactions, mode conversion) can inject energy for turbulence. Electromagnetic turbulence has indeed been observed in the magnetopause (e.g., LaBelle & Treumann, 1988; Rezeau & Belmont, 2001), and is suggested to be a key ingredient for diffusive particle transport across the magnetopause (e.g., Johnson & Cheng, 1997; Lin et al., 2012). However, the origin of electromagnetic fluctuations in the magnetopause and its boundary layers remains unclear, because various processes, such as magnetopause reconnection (Chaston et al., 2005), the KHI (Daughton et al., 2014; Nakamura, Hasegawa, et al., 2017), and mode conversion at the magnetopause of magnetosheath compressional fluctuations (Johnson & Cheng, 1997; Johnson et al., 2001), can inject energy for the magnetopause turbulence.

In the present study, we investigate the generation process of electromagnetic turbulence in magnetopause Kelvin-Helmholtz (KH) vortices by analyzing high-resolution plasma and electromagnetic field data taken in situ by the Magnetospheric Multiscale (MMS) spacecraft (Burch et al., 2016). For this purpose, we revisit a KH event observed by MMS on 8 September 2015 under northward interplanetary magnetic field (IMF) conditions. Identified in this event are magnetic reconnection induced by the KHI growth because of the presence of weak but significant magnetic shears across the magnetopause (Eriksson et al., 2016; Li et al., 2016; Vernisse et al., 2016; Nakamura, Hasegawa, et al., 2017), turbulence in both flow and electromagnetic fields and its intermittent nature (Stawarz et al., 2016), and large-amplitude electrostatic waves (Wilder et al., 2016). Intermittency in the turbulence context means that energy transfer across length scales is spatially nonuniform, for example with localization in current sheets or filaments (e.g., Matthaeus et al., 2015). While the KHI itself could have injected most energy for the turbulence as observed, it is possible that magnetopause reconnection poleward of the cusp under northward IMF (e.g., Lavraud et al., 2006; Øieroset et al., 2008) also played some role in the turbulence generation (Chaston et al., 2005; Nykyri et al., 2006). Indeed, in the MMS KHI event, there is evidence that a prominent low-latitude boundary layer (LLBL) formed through magnetopause reconnection exists on the earthward side of the KH-active magnetopause (Nakamura, Eriksson, et al., 2017).

In this paper, the following questions are addressed. What are the relative contributions of high-latitude magnetopause reconnection and the KHI to the turbulence generation in the KH vortices? What is the mode of the observed electromagnetic fluctuations; are they of propagating normal mode waves or something else? Could the electromagnetic turbulence play a role in plasma transport across the magnetopause? Section 2 presents overviews of the MMS event on 8 September 2015 with both KHI and reconnection signatures and of another magnetopause event

with reconnection but no KHI signatures. In section 3, magnetic energy spectra are compared between the MMS observations with and without KHI signatures, and between the MMS observations and fully kinetic simulations of the KHI, to answer the question of the relative contributions. In section 4, a technique to estimate wave number vectors is used to analyze the mode of the turbulent fluctuations. In section 5, a discussion is given on the generation process of the turbulence and the causality between the turbulence and plasma transport across the magnetopause. Conclusions are provided in section 6.

2 Overview of Events with and without Kelvin-Helmholtz Signatures

2.1 Kelvin-Helmholtz event on 8 September 2015

Figure 1 shows data of our interest, from the fluxgate magnetometer (FGM) (Russell et al., 2016) and the Fast Plasma Investigation (FPI) instrument (Pollock et al., 2016) onboard the MMS3 spacecraft for a 2.5-hour interval 0910–1140 UT on 8 September 2015, during which MMS traversed the magnetopause boundary layers from the postnoon magnetosphere into the duskside magnetosheath. On this day, an interplanetary magnetic flux rope was passing by the Earth and brought about northward IMF conditions in front of the magnetosphere (Eriksson et al., 2016). The average solar wind conditions for the interval 1030–1100 UT based on the OMNIWeb data, which are time shifted to the bow shock nose, are: IMF (B_x, B_y, B_z) = (13.2, 6.0, 14.9) in GSM, solar wind speed 506 km/s, solar wind density 10.6 cm^{-3} , plasma beta 0.15, and magnetosonic Mach number 3.7. See Figure S1 for the time history of the upstream conditions over a long time period, showing that the solar wind parameters were stable for the interval shown in Figure 1. MMS observed quasi-periodic fluctuations of the plasma bulk parameters with a period ~ 1 min (corresponding to the KHI wavelength $\sim 10^4$ km), associated with the KHI, during the interval enclosed by the red box in Figure 1 when the spacecraft were located at or near the duskside magnetopause. Based on a detailed comparison between the MMS observations and three-dimensional (3D), fully kinetic simulations of the KHI, Nakamura, Hasegawa, et al. (2017) showed that the KHI at the MMS location was in an early nonlinear phase when vortex induced reconnection (VIR) (Nakamura et al., 2011; 2013) forms jets and vortices with filamentary density structures of ion scales.

A dense boundary layer existed for an interval 0930–1005 UT prior to the KH-active period (Figure 1a,d). This boundary layer lacked hot magnetospheric electrons with energies ~ 5 keV and contained heated magnetosheath electrons with energies of a few hundred eV, and thus likely formed through double high-latitude reconnection that can capture magnetosheath particles onto the closed portion of the dayside magnetosphere (Song & Russell, 1992; Øieroset et al., 2008). Northward increases of the boundary layer ion velocity relative to the magnetosheath flow, seen during the KH-active interval (Figure 1c), are probably due to acceleration resulting from magnetopause reconnection poleward of the southern cusp. Note that MMS was in the southern hemisphere ($z_{\text{GSM}} \sim -5 R_E$), closer to the southern than northern cusp. The presence of the dense boundary layer lowers the threshold for the KHI, and most likely made the KHI onset location closer to the subsolar point than in the case without boundary layer (Hasegawa, Retinò, et al., 2009; Nakamura, Eriksson, et al., 2017). Hereafter, this event is referred to as the RX+KHI event because both the poleward-of-the-cusp reconnection and KHI signatures were observed.

Low frequency fluctuations of the magnetic field were observed during the KH-active interval (Figure 1f). Large-scale variations with a quasi-period ~ 1 min (~ 0.02 Hz) are consistent

with 3D deformation of field lines expected at the MMS location in the southern hemisphere through the KHI in the magnetospheric flank geometry (Hasegawa et al., 2004; Hasegawa, Retinò, et al., 2009). This deformation probably allowed for KHI-induced mid-latitude reconnection (Faganello et al., 2012; Fadanelli et al., 2018), whose particle signatures were reported by Vernisse et al. (2016). Magnetic power spectra in Figure 1g,h show that the fluctuations are seen in the frequency range from the KHI fundamental mode (~ 0.02 Hz) to higher than the proton cyclotron frequency (~ 1 Hz). Obviously, the fluctuations during the KH-active and preceding boundary layer intervals are more intense than in the surrounding magnetosheath and magnetospheric regions, suggesting that they originated from the KHI. While considerable compressional components are present (Figure 1g), the fluctuations are dominated by the transverse components (Figure 1h).

2.2 Subsolar magnetopause event on 8 November 2015

Figure 2 shows an event on 8 November 2015 when MMS traversed the subsolar magnetopause under northward IMF. The average solar wind conditions for the interval 0630–0700 UT are: IMF $(B_x, B_z, B_y) = (-8.6, 4.7, 6.0)$ in GSM, solar wind speed 478 km/s, solar wind density 2.6 cm^{-3} , plasma beta 0.12, and magnetosonic Mach number 3.2. See Figure S2 for the upstream conditions over a long time interval, showing that this event also occurred when an interplanetary flux rope interacted with the magnetosphere. The external conditions are thus similar to the case on 8 September 2015 in that IMF $|B_z| > |B_y|$, and the solar wind speed, beta, and Mach number are all comparable. This event, with high-latitude reconnection but without KHI signatures as demonstrated below, was selected to compare with the RX+KHI event encountered farther from the subsolar point, and to differentiate the KHI and high-latitude reconnection effects on the magnetic turbulence generation. During the interval shown in Figure 2, MMS moved from the magnetosheath into the LLBL with densities comparable to that in the magnetosheath. Because of the strong northward IMF, the magnetopause current sheet cannot be identified from the magnetic field data (Figure 2a,b) (Hasegawa, 2012). However, ion temperature increase and anisotropy variation at ~ 0634 UT from $T_{i\perp} > T_{i\parallel}$ to $T_{i\perp} \sim T_{i\parallel}$ (Figure 2c) indicate that a crossing from the magnetosheath to the LLBL occurred (Paschmann et al., 1993). Contrary to observations as reported by Sahraoui et al. (2006), mirror-mode structures were not observed on the magnetosheath side (not shown) likely because of the low beta upstream conditions (Figure S2).

The observed magnetosheath boundary layer (MSBL) and LLBL had clear signatures of reconnection poleward of the southern cusp. The northward component of the ion velocity increased from near zero to ~ 100 km/s at $\sim 0634:20$ UT (Figure 2d), consistent with northward acceleration of magnetosheath ions in downstream regions equatorward of the southern cusp reconnection site. Ion velocity distributions observed in the LLBL (Figure 2h) show preexistent magnetosheath populations with $T_{i\perp} > T_{i\parallel}$ and D-shaped accelerated components with a magnetic field-aligned cutoff velocity at 300–400 km/s (Fuselier, 1995). In addition, energy dispersed ions consistent with the velocity filter effect (Figure 2e) and 0.2–2 keV electrons streaming parallel to the magnetic field, consistent with heating of magnetosheath electrons in regions southward of MMS (Figure 2g), were observed during the MSBL interval (before $\sim 0634:20$ UT). While bidirectional electron populations in the LLBL (Figure 2g,i) suggest that the magnetospheric side may be closed through double poleward-of-the-cusp reconnection

(Øieroset et al., 2008), particle signatures of southern, rather than northern, cusp reconnection were prominent in the MSBL and at the magnetopause. This is probably because there was a substantial geomagnetic dipole tilt on this day and thus MMS was closer to the southern cusp, namely, the high-latitude reconnection site in the summer hemisphere (Hasegawa, McFadden, et al., 2009). This event is referred to as the RX-only event because no KHI but only reconnection signatures were identified. We note that MMS saw fluctuations of the ion velocity as well as the magnetic field in the LLBL (Figure 2a,d), whose spectral properties and mode are analyzed in sections 3 and 4.

3 Power Spectral Analysis

3.1 Comparison between the dayside reconnection and KHI events

Magnetic power spectra in the LLBL are compared for the RX+KHI and RX-only events in order to discuss the origin of the magnetic turbulence at magnetohydrodynamic (MHD) and ion scales observed in KH vortices. Figure 3 shows the power spectral densities (PSDs) of the field intensity $|\mathbf{B}|$ and transverse component B_n normal to the magnetopause for the two events. For the RX+KHI event, a total of 51 LLBL intervals during the KHI-active period were identified by visual inspection (see Table S1 for the exact time intervals) and were used to produce the mean PSDs, excluding the magnetosheath intervals and apparently reconnecting magnetopause current sheets, as reported by Eriksson et al. (2016). Here, the normal \mathbf{n} is defined to be parallel to the cross product of the mean ion velocity $\langle \mathbf{v}_i \rangle$, which is tailward roughly along the magnetopause for KH events (Hasegawa et al., 2006), and mean magnetic field $\langle \mathbf{B} \rangle$ for each interval. The frequency can be converted to the perpendicular wave number and vice versa using the Taylor hypothesis $2\pi f_{sc} = \mathbf{k}_\perp \cdot \langle \mathbf{v}_{i\perp} \rangle$, with the mean perpendicular ion velocity $\langle \mathbf{v}_{i\perp} \rangle = 203$ km/s for the RX+KHI event and $\langle \mathbf{v}_{i\perp} \rangle = 76$ km/s for the RX-only event. We will confirm in sections 4.2 and 4.3 that the Taylor hypothesis is valid at frequencies <10 Hz for the two events under discussion. With this conversion, Figure 3 also shows the spatial scales $k_\perp \rho_p = 1$ and $k_\perp d_p = 1$, corresponding to the thermal proton gyroradius $\rho_p \sim 45$ km and proton inertial length $d_p \sim 65$ km, respectively, averaged over the 51 intervals for the RX+KHI event, and $\rho_p \sim 79$ km and $d_p \sim 94$ km for the RX-only event.

The PSD levels for both $|\mathbf{B}|$ and B_n are higher for the RX+KHI event than for the RX-only event for almost the entire frequency range. For comparison, we take into account the fact that the background field intensity for the RX+KHI case (~ 70 nT in Figure 1f) was about twice that for the RX-only event (~ 40 nT in Figure 2a). If the turbulence field was quasi-2D and the flux tubes in which the turbulence was embedded were advected and compressed from the subsolar location of the RX-only event to that of the RX+KHI event, the expected PSD level would be ~ 4 times that seen in Figure 3b. However, the PSD of B_n is about one order of magnitude, i.e., more than four times, larger in Figure 3a than in Figure 3b. This suggests that while high-latitude reconnection can inject a modest amount of energy into turbulence at low latitudes, the KHI further amplifies the turbulence.

There are interesting differences in the spectral features between the RX+KHI and RX-only events. While the PSDs of $|\mathbf{B}|$ and B_n are comparable in the RX-only event, the B_n energy density is significantly higher than that of $|\mathbf{B}|$ in the RX+KHI event (Stawarz et al., 2016). At lower (MHD-scale) frequencies, the spectral index $-5/3$ for both $|\mathbf{B}|$ and B_n for the RX+KHI

event is consistent with the Kolmogorov or Goldreich-Sridhar model (Goldreich & Sridhar, 1995). In the higher frequency range, the index for B_n gradually decreases with frequency and becomes smaller than -3 , while that for $|\mathbf{B}|$ is in the range of -3 to $-8/3$, similar to those reported by Stawarz et al. (2016). For the RX-only event, while the fluctuations at frequencies higher than the proton cyclotron frequency f_{cp} follows $f_{sc}^{-8/3}$ for both $|\mathbf{B}|$ and B_n , the B_n spectrum only has a clear peak immediately below f_{cp} . In section 4.3, it is shown that this intense transverse fluctuation is of electromagnetic ion-cyclotron (EMIC) waves.

3.2 Comparison between the KHI observation and simulation

3D fully kinetic simulations of the KHI conducted specifically for the RX+KHI event, as reported by Nakamura, Hasegawa, et al. (2017), Nakamura, Eriksson, et al. (2017), and Nakamura (2019), are compared with the MMS KHI observations in terms of spectral properties of magnetic turbulence. The initial conditions of the simulations are set based on the parameters observed in the magnetosheath- and LLBL-side regions of the KH-active magnetopause, with the initial magnetic shear $\sim 17^\circ$ and the LLBL to magnetosheath density ratio of 0.3 (see the Methods section of Nakamura, Hasegawa, et al. (2017) for details), but no broadband magnetic field or velocity fluctuations are imposed. This means that effects of turbulence that may exist in the magnetosheath and/or LLBL before the KHI onset are not included in the simulations. Figure 4 shows energy spectra of $|\mathbf{B}|$ and the field component B_y normal to the initial velocity shear layer, corresponding to B_n in the MMS observations, in an early nonlinear phase ($t = 500\Omega_i^{-1}$) and more developed phase ($t = 700\Omega_i^{-1}$) of the KHI. We point out that B_y at ion to sub-ion scales roughly corresponds to reconnected field components generated by VIR (Nakamura et al., 2011; 2013), though B_y at MHD scales results from large-scale evolution of KH vortices.

Nakamura, Hasegawa, et al. (2017) showed that the KHI in the RX+KHI event was in an early nonlinear phase, as shown in Figure 4a, when VIR was growing and formed ion-scale vortices along the interface (magnetopause) between the dense (magnetosheath) and less dense (LLBL) plasmas. At the MHD scales, the PSD of B_y is about one order of magnitude higher than that of $|\mathbf{B}|$, in agreement with the MMS observations (Figure 3a). However, the spectral index at $t = 500\Omega_i^{-1}$ is smaller than $-5/3$ seen in the observations, suggesting that the turbulence is still growing in the simulation. The observed spectral indices are rather similar to those in a more developed phase of the simulation (Figure 4d) when the plasmas are vigorously mixed within the MHD-scale vortex (Figure 4c) and the turbulence is matured. The comparison suggests that in the observed KH vortices, turbulence matured faster than in the simulation. It may be that the preexisting magnetosheath turbulence (Alexandrova et al., 2008) and/or turbulence in the LLBL generated through magnetopause reconnection (Chaston et al., 2005) contributed to faster maturation of turbulence in the observed KH vortices (Nakamura et al., 2019).

4 Dispersion Relation Analysis

4.1 Bellan's method to estimate wave vectors

A single-spacecraft method to estimate the wave vector of magnetic field fluctuations, developed by Bellan (2012, 2016), is used to reveal the mode of the observed turbulence. The technique is based on Ampère's law and makes use of the condition that the k-vector of low-

frequency waves should be parallel to $\delta \mathbf{j} \times \delta \mathbf{B}$, where $\delta \mathbf{j}$ and $\delta \mathbf{B}$ are the fluctuating components of the current density and magnetic field. More exactly, wave vectors $\mathbf{k}(\omega_{sc})$ as a function of spacecraft frequency are given by

$$\mathbf{k}(\omega_{sc}) = i\mu_0 \frac{\mathbf{j}(\omega_{sc}) \times \mathbf{B}^*(\omega_{sc})}{\mathbf{B}(\omega_{sc}) \cdot \mathbf{B}^*(\omega_{sc})}, \quad (1)$$

where $\mathbf{j}(\omega_{sc})$ and $\mathbf{B}(\omega_{sc})$ are the temporal Fourier transforms of the current density $\mathbf{j}(t)$ and magnetic field $\mathbf{B}(t)$, respectively, and $\mathbf{B}^*(\omega_{sc})$ is the complex conjugate of $\mathbf{B}(\omega_{sc})$ (see equation (8) of Bellan, 2016). It assumes that the displacement current is negligible, i.e., the charge quasi-neutrality is satisfied, and that there exists only one mode for a given frequency in the spacecraft frame and the fluctuations or waves are planar. While the method was first applied to MMS magnetometer measurements of $\delta \mathbf{B}$ and $\nabla \times \mathbf{B}/\mu_0$ in kinetic Alfvén waves (KAWs) propagating in a magnetopause boundary layer (Gershman et al., 2017), it can also take advantage of unprecedented high resolution ion and electron measurements by FPI that provide high cadence (30 ms) data of the current density $\mathbf{j} = ne(\mathbf{v}_i - \mathbf{v}_e)$. Applications to particle current data were made by Gershman et al. (2018) who analyzed kinetic scale turbulence in the magnetosheath. Recently, Haw et al. (2019) applied this method to identify whistler waves in a laboratory experiment of magnetic reconnection.

The method provides information similar to that obtained from the k-filtering method (Pinçon & Lefeuvre, 1991) or equivalent wave telescope technique (Neubauer & Glassmeier, 1990; Narita, Plaschke, et al., 2016), making use of at least four point measurements of the magnetic field. A key difference is that the k-filtering and wave telescope methods permit the presence of more than one mode (k-vectors) for a given frequency in the spacecraft frame. In theory, the assumption in Bellan's method of only one mode for a given frequency prohibits application to isotropic or gyrotropic turbulence in which there would be many k-vectors with different directions for a given frequency. Nonetheless, Gershman et al. (2018) demonstrated that the Bellan and k-filtering methods provide roughly equal wave vectors for broadband low frequency fluctuations (<3 Hz in the spacecraft frame) observed in the magnetosheath. For the RX+KHI event, the MMS spacecraft separation was ~175 km, much larger than the proton gyroradius ~45 km, so that the wave telescope or k-filtering technique could not be used to analyze turbulence properties around ion scales, which are of our interest.

We emphasize that all the above methods do not necessarily provide wave vector(s) in the plasma rest frame, but information on the direction in which the waves or structures are propagating in the spacecraft frame. To derive the plasma-frame k-vector, the Doppler effect must be taken into account. If $\mathbf{k} \cdot \mathbf{u}_0 < 0$, where \mathbf{k} is the k-vector derived from the above methods and \mathbf{u}_0 is the ambient plasma flow velocity, \mathbf{k} would be the true wave vector in the plasma-rest frame. If $\mathbf{k} \cdot \mathbf{u}_0 > 0$ and the plasma frame angular frequency $\omega_{pl} = \omega_{sc} - \mathbf{k} \cdot \mathbf{u}_0 > 0$, where ω_{sc} is the frequency in the spacecraft frame, the wave should be propagating along \mathbf{u}_0 and the derived k-vector \mathbf{k} would be the plasma-frame wave vector, while if $\mathbf{k} \cdot \mathbf{u}_0 > 0$ and $\omega_{pl} < 0$, the true wave vector should have a component antiparallel to \mathbf{u}_0 and thus the sign of \mathbf{k} should be reversed to derive the plasma-frame wave vector (Narita et al., 2011).

4.2 Wave vector properties

Figure 5 shows an example interval in the RX+KHI event to which Bellan's method is applied. We apply the method to boundary layer intervals on the magnetospheric side of the magnetopause, as marked by the red box in Figure 5, which exclude thin current sheets at the trailing edges of the KHI surface waves (Eriksson et al., 2016; Stawarz et al., 2016) and can be assumed to be of quasi-homogeneous plasma. Electric field data (Figure 5b) are from the spin-plane and axial probes measurements (Ergun et al., 2016; Lindqvist et al., 2016), and Poynting flux $\mathbf{S} = \delta\mathbf{E} \times \delta\mathbf{B}/\mu_0$ (Figure 5h) is computed in the ion-rest frame where $\delta\mathbf{E} = \mathbf{E} + \langle\mathbf{v}_i\rangle \times \langle\mathbf{B}\rangle$ and $\delta\mathbf{B} = \mathbf{B} - \langle\mathbf{B}\rangle$. Here \mathbf{E} is the electric field in the spacecraft frame, and $\langle\mathbf{v}_i\rangle$ and $\langle\mathbf{B}\rangle$ are 4-sec running averages of the ion velocity and magnetic field, respectively. For the RX-only event, Bellan's method is applied to the interval 0635:10–0635:40 UT on 8 November 2015, as marked in Figure 2.

Figure 6 shows four-spacecraft averages of the \mathbf{k} -vector directions and the k magnitude as a function of the spacecraft frequency f_{sc} (up to 7 Hz), derived from Bellan's method, for the RX+KHI and RX-only events. A Hanning window was used when performing Fast Fourier Transforms (FFTs), following the procedure taken by Gershman et al. (2018). Figure 6 has gaps in certain frequency ranges, because the results are restricted to cases when for a given spacecraft frequency f_{sc} , the four \mathbf{k} -vectors, derived individually for each spacecraft, all have angles less than 35° with respect to the four-spacecraft average.

For both the RX+KHI and RX-only events, the estimated wave vectors are nearly perpendicular to the background magnetic field (Figure 6b,f), mostly have a component along the ambient ion flow (Figure 6c,g), and roughly satisfy the Taylor hypothesis $2\pi f_{sc} = k\langle v_i\rangle\cos(\theta_{kv})$ (Figure 6d,h). The last point indicates that the turbulence fields roughly convect at the mean flow velocity, so that the spacecraft frequency f_{sc} may be converted to the wave number using the linear relation. Here, the mean field in GSM is directed along $\langle\mathbf{b}\rangle = (0.160, 0.581, 0.798)$ and the mean ion velocity $\langle\mathbf{v}_i\rangle = (-132, 161, -26)$ km/s for the RX+KHI event, and $\langle\mathbf{b}\rangle = (0.321, 0.272, 0.907)$ and $\langle\mathbf{v}_i\rangle = (31, 109, 111)$ km/s for the RX-only event. Similar features have been reported for turbulence in the solar wind (Narita et al., 2011; Sahraoui et al., 2010) and in the magnetosheath (Gershman et al., 2018). One exception is a few \mathbf{k} -vectors at and below the proton cyclotron frequency f_{cp} for the RX-only event, which have propagation angles $\sim 45^\circ$ with respect to the magnetic field. Note that the transverse magnetic field fluctuations had a significant power around f_{cp} (Figure 3b). In section 4.3, we identify these fluctuations as of the slow (EMIC) mode.

To make sure that the results as shown in Figure 6 are reasonable, Bellan's method has also been applied to synthetic data taken by a virtual spacecraft passing through a simulated 3D KH vortex in a nonlinear phase, corresponding to the one shown in Figure 4c. It is found that the \mathbf{k} -vector properties derived from the simulated data are very similar to those seen in the RX+KHI event, as shown in Figure 6a-d (see the Supporting Information). We also note that results similar to those shown in Figure 6a-d were obtained for other LLBL intervals in the RX+KHI event.

4.3 Dispersion relations

Using $\mathbf{k}(\omega_{sc})$ estimated by Bellan's method, the dispersion relation $\omega_{pl}(\mathbf{k})$ and parallel phase velocity $\omega_{pl}(\mathbf{k})/k_{\parallel}$ in the plasma-rest frame can be derived by taking the Doppler shift

into account, $\omega_{pl} = \omega_{sc} - \mathbf{k} \cdot \mathbf{u}_0$. Figure 7 shows the parallel phase velocities $\omega_{pl}(\mathbf{k})/(k_{\parallel}v_A)$ normalized to the MHD Alfvén speed, and $\omega_{pl} - k$ diagrams for the two intervals, derived from the four-spacecraft averages as shown in Figure 6. Here, $v_A = 477$ km/s, $\Omega_p = eB/m_p = 7.61$ rad/s, proton gyroradius $\rho_p = 44$ km, and plasma beta $\beta = 0.46$ for the RX+KHI event, and $v_A = 361$ km/s, $\Omega_p = 3.86$ rad/s, $\rho_p = 80$ km/s, and $\beta = 0.72$ for the RX-only event. The error bars in Figure 7b,d are based only on the standard deviations σ_v of the ion velocity component along \mathbf{k} during the intervals, which are ~ 60 km/s for the RX+KHI event and ~ 30 km/s for the RX-only event. Error magnitudes based only on the standard deviations of the component along the average ion velocity ($\langle \mathbf{v}_i \rangle = \mathbf{u}_0$) of the four \mathbf{k} -vectors (each from each spacecraft) are comparable to those in Figure 7b,d.

Curves in Figure 7 show theoretical linear dispersion relations for the fast (magnetosonic-whistler), kinetic Alfvén, and slow (EMIC) modes based on the two-fluid model, i.e., exact solutions of equation (29) derived by Bellan (2012) (see section 5 of their paper), for three propagation angles $\theta = 49^\circ$, 69° , and 89° with respect to the magnetic field. For the RX+KHI event, the data points are distributed around $\omega_{pl} = 0$, and do not appear to collectively satisfy any of the theoretical dispersion relations. On the other hand, for the RX-only event many points are near the slow-mode curve, especially at smaller k ($k < 0.1$ rad/km), while other points are distributed around $\omega_{pl} = 0$. It can be concluded that the magnetic turbulence in the RX+KHI event is not made of propagating normal-mode waves, but fossil magnetic field structures with transverse fluctuating components were advected by the background plasma flow. On the other hand, the EMIC mode was an ingredient of the fluctuations in the RX-only event.

We do not discuss details of the excitation process of the EMIC waves in the RX-only event, which is not the focus of our study. Since they were propagating northward along the magnetic field (Figure 6e,f), it is possible that they were generated closer to the reconnection site near the southern cusp. We note, however, that the ion beam streaming along the magnetic field, as seen in Figure 2h, would not be the driver of the waves, because EMIC waves can grow when the ion beam travels in the direction opposite to the wave propagation (Ahirwar et al., 2007).

5 Discussion

5.1 Generation process of the KHI driven turbulence

Our results suggest that while magnetic reconnection at the high-latitude magnetopause excites a modest level of magnetic turbulence in the dayside low-latitude boundary layer (Figure 3b), the KHI further amplifies the turbulence with the transverse magnetic energy significantly higher than the compressional energy (Figure 3a). Similar results have been obtained for simultaneous observations on 20 November 2001 of the dayside magnetopause with reconnection signatures and the dusk-flank magnetopause with active KHI signatures, reported by Hasegawa, Retinò, et al. (2009). The spectral indices $-5/3$ at MHD scales and about -3 at sub-ion scales have also been seen in other KHI events (Di Mare et al., 2019), and are consistent with 2D kinetic simulations of magnetic turbulence (Franci et al., 2017) as well as 3D kinetic simulations of the KHI (Nakamura, Hasegawa, et al., 2017). The transverse components of sub-ion-scale magnetic field fluctuations roughly corresponds to the reconnected field components and, notably, both kinetic simulations and observations show that magnetic reconnection can

produce magnetic turbulence with the spectral index of about $-8/3$ at sub-ion scales (Daughton et al., 2014; Eastwood et al., 2009), consistent with the present observations.

It should be stressed that power-law magnetic spectra with a spectral index $-5/3$ in the MHD range, as expected for a quasi-steady turbulence, were observed even in the early nonlinear phase (at $1-2$ eddy turnover time $\pi\alpha^{-1} = \pi\lambda_{\text{KHI}}/V_0$) of the KHI, corresponding to the stage as shown in Figure 4a. What could be the process for such fast turbulence generation? Recent kinetic simulations of the KHI show that if modest magnetic field fluctuations, as seen in Figure 3b, are present in the magnetopause before the KHI onset, magnetic turbulence with a spectral index $-5/3$ can be generated even in the early nonlinear stage (T. K. M. Nakamura, private communication, 2019).

We also note that energy cascade in KH vortices may be proceeding through the process, as suggested by Franci et al. (2017), in which magnetic reconnection may act as a rectifier to directly transfer energy from MHD scales to sub-ion scales, rapidly driving sub-ion-scale energy cascade. In such situations, energy injected at MHD scales can be transferred to smaller scales not only gradually via standard direct cascade but also rapidly via reconnection that occurs in sub-ion-scale current sheets. Their results are interesting in that cross-scale energy transfer in turbulence may occur via magnetic reconnection (see Figure 4 of Franci et al., 2017), while conventional wisdom is that energy cascade at MHD scales occurs via nonlinear interactions of vortices or counter-propagating Alfvén waves. In the case of the KHI with an initial magnetic shear or magnetic field deformation involved (Nakamura et al., 2006; Nykyri & Otto, 2001), MHD dynamics (vortical flow) produces thin current sheets subject to magnetic reconnection and, as a result of VIR, part of energy at MHD scales may be directly transferred to sub-ion scales, and forward and inverse cascades at kinetic scales may set in.

Both of the two MMS events studied in the present paper were observed when an interplanetary flux rope passed by the Earth, i.e., when the upstream plasma beta and Alfvén Mach number were both rather low (Figures S1 and S2). However, KH waves/vortices can be observed under other upstream conditions (Lin et al., 2014; Kavosi & Raeder, 2015) and the generation mechanism of turbulence may be different for different conditions. In particular, the magnetosheath is often turbulent with mirror-mode structures (e.g., Sahraoui et al., 2006) under high beta conditions and preferentially in the downstream of quasi-perpendicular shocks (Soucek et al., 2015), and with substantial velocity fluctuations under high Mach number conditions and preferentially in the downstream of quasi-parallel shocks (Nykyri et al., 2017). The effects of these magnetosheath structures and fluctuations on boundary layer turbulence are not fully understood and should be investigated in the future.

5.2 Mode of the KHI driven turbulence

The nature of electromagnetic field fluctuations in KH vortices is discussed in detail. The analysis in section 4 suggests that the magnetic turbulence in KH vortices does not satisfy any linear dispersion relation for propagating normal-mode waves, and thus consists of magnetic structures of various scales being advected by the background bulk flow ($\omega_{\text{pl}} \sim 0$). The \mathbf{k} -vectors roughly perpendicular to the background field (Figure 6b) indicates that the magnetic structures with transverse field fluctuations (Figure 3a) have boundaries or inhomogeneity roughly in the perpendicular direction, i.e., the turbulence consists of weakly curved magnetic flux tubes of various scales. We note that such flux tubes can be produced in KH vortices through multiple VIR and become interlaced in the nonlinear phase (see Figure 6 of Nakamura et al. (2013)). Such

a filamentary or “spaghetti-like” flux tubes picture has been suggested and demonstrated for turbulence in the solar wind (Borovsky, 2008; Hu et al., 2018), at least part of which would be driven by convective fluid motions on the photosphere.

A caveat is that the assumptions underlying Bellan’s method of plane waves or planar structures and one mode for a given spacecraft frequency may well be violated in KH vortices. Indeed, Figure 5h,i shows that both Poynting flux and the normalized cross helicity, the latter of which can be used as a measure of Alfvénicity of MHD turbulence and to infer the propagation direction in the plasma frame of Alfvén waves, intermittently have significant positive or negative values during the analyzed and other intervals. It suggests that counter-propagating Alfvén waves may be embedded in KH vortices. Here, the normalized ion cross helicity is defined as $\sigma_{ci} = H_{ci}/E_i$, where the ion cross helicity $H_{ci} = \langle \mathbf{v}_i \cdot \mathbf{b} \rangle$, average energy $E_i = \langle v_i^2 + b^2 \rangle / 2$, and the magnetic field \mathbf{b} is expressed in Alfvén units $\mathbf{B} / \sqrt{\mu_0 \rho_p}$ (Bruno & Carbone, 2013).

With the possibility of counter-propagating waves in mind, we have analyzed energy spectra of electric field fluctuations and the ratio between the normal component of the fluctuating electric field and the tangential component of the fluctuating magnetic field, as shown in Figure 8. Here the normal is $\mathbf{n} = (0.705, 0.499, -0.504)$ in GSM, and the tangential direction is defined as $\mathbf{t} = \langle \hat{\mathbf{b}} \rangle \times \mathbf{n} = (-0.691, 0.643, -0.330)$. The ratio is equivalent to the parallel phase velocity of the waves, when the wave vectors are in the plane containing $\langle \hat{\mathbf{b}} \rangle$ and \mathbf{t} . This may well be the case because the \mathbf{k} -vectors from Bellan’s method are roughly along the mean flow velocity \mathbf{u}_0 which is in the $\langle \hat{\mathbf{b}} \rangle - \mathbf{t}$ plane (Figure 6b,c). Here, the measured electric field is converted to that in the mean flow frame, $\mathbf{E}' = \mathbf{E} + \mathbf{u}_0 \times \mathbf{B}$. Figure 8b shows that the transverse component of \mathbf{E}' is dominated by that $-\delta \mathbf{v}_e \times \mathbf{B}_0$, which is because the amplitude of the magnetic field fluctuations $\delta \mathbf{B}$ during the boundary layer interval is considerably smaller than $|\mathbf{B}_0|$ (Figure 5a).

The amplitude of δE_n being larger than that of δE_t may be due to electron jets from VIR being roughly directed in the tangential direction, i.e., $|\delta v_{et}|$ larger than $|\delta v_{en}|$. Interestingly, Figure 8c shows that both $\delta E_n / \delta B_t$ and $\delta E_t / \delta B_n$ roughly satisfy the linear dispersion relation of KAWs with $\theta = 89^\circ$, the propagation angle compatible with the observed \mathbf{k} -vector directions (Figure 6b), and using the Taylor hypothesis. This may indicate that KAWs were a constituent of the electromagnetic turbulence observed in the KH vortices. However, $|\delta E_n| > |\delta E_t|$ (Figure 8b) suggests that the wave vectors had larger normal, rather than tangential, components if KAWs are involved (Hollweg, 1999; Bellan, 2012; Lin et al., 2012). In fact, if KAWs are emitted by VIR, it is reasonable to suppose that the wave vectors point mostly in the normal, rather than tangential, direction, as in the case of MHD Alfvén waves (rotational discontinuities) emitted from reconnecting current sheets. We also point out that the KAW modes with wave vectors mostly along the normal cannot simply result from mode conversion from the KH waves (Chaston et al., 2007), because KH waves have wave vectors roughly in the tangential direction.

How could these seemingly contradictory results be reconciled? One possibility is that the electromagnetic fluctuations in the KH vortices are in a strongly turbulent state, and thus do not satisfy the properties of linear modes, such as linear dispersion relations. It is also possible that since magnetic reconnection can excite KAWs in outflow regions (Chaston et al., 2005) and VIR in 3D can occur at various latitudinal locations (Vernisse et al., 2016; Nakamura, Hasegawa, et al., 2017; Nakamura, Eriksson, et al., 2017; Fadanelli et al., 2018), KAWs propagating in opposite directions are embedded and interacting in the KH vortices. Indeed, magnetic flux ropes observed in association with the KH-active magnetopause (Eriksson et al., 2009; Sturmer et al.,

2018) are signatures of such multiple reconnection in KH vortices, and may actually be interlaced flux tubes in 3D. Notably, the interlaced field lines with filamentary currents in the KH vortices may be the origin of intermittent features of the turbulence, as reported by Stawarz et al. (2016). We also point out that the presence of positive and negative ω_{pl} (Figure 7a,b) may be interpreted as a signature of waves/structures having \mathbf{k} -vector components parallel and antiparallel to \mathbf{u}_0 in the plasma-rest frame. However, since the FFT-based Bellan method allows only one mode for a given spacecraft frequency and selected interval, the turbulence as a whole may manifest as magnetic structures advected by the bulk flow in the KH vortices. Future studies using Bellan's method should probably use more advanced spectral analysis, such as wavelet transforms, to derive instantaneous wave vectors.

The possibility that VIR could excite KAWs indicates that there may be a new path to locally generate KAW turbulence in the magnetopause boundary layer, in addition to the paths through dayside magnetopause reconnection (Chaston et al., 2005) and resonant mode conversion from magnetopause surface or KH waves (Hasegawa, 1976; Chaston et al., 2007) or from magnetosheath compressional waves (Johnson & Cheng, 1997; Lin et al., 2010). The role of such VIR driven KAWs is unknown and needs to be explored in the future.

While the possible contribution of KAWs to turbulence in KH vortices was discussed here, EMIC and/or magnetosonic waves may also be observed in other cases. Moore et al. (2016) indeed identified magnetosonic waves inside KH vortices observed on the dawn side and discussed their role in ion heating. Such waves may be excited in KH vortices when cool magnetosheath and hot magnetospheric ions are spatially mixed, or when energetic ions of plasma sheet origin drift into the boundary layer, forming a ring distribution. On the other hand, ion velocity distributions in and around KH vortices would be stable for ion cyclotron anisotropy instabilities, with the parallel temperature often higher than the perpendicular temperature (Nishino et al., 2007). Thus, EMIC waves may be damped quickly in the flank boundary layer even if they exist or are excited in the cusp (Nykyri et al., 2006) or in the dayside boundary layer (section 4.3). Further study would be needed to reveal the contribution of these waves.

5.3 Role of the KHI driven turbulence

Earlier observations demonstrated that magnetic reconnection can be induced locally at the KH-unstable magnetopause and remotely at mid-latitudes as a consequence of the KHI (Eriksson et al., 2016; Nakamura, Hasegawa, et al., 2017; Vernisse et al., 2016). Simulation studies (Nakamura, Hasegawa, et al., 2017; Nakamura, Eriksson, et al., 2017) also show that VIR in 3D can cause an efficient plasma mixing and drive magnetic turbulence with a power-law index $-8/3$ at sub-ion scales as observed. Combined with such results, our results suggest that the sub-ion-scale turbulence in the early nonlinear phase of the KHI is a consequence of VIR, the primary plasma transport process at this stage.

If KAW turbulence could be excited through VIR (Figure 8c), one may think that particle diffusion induced by KAWs could play an additional role in the transport across the magnetopause (Johnson & Cheng, 1997; Izutsu et al., 2012), in particular if the KAW turbulence is further amplified in more downstream regions. However, the KAW mode with $|\delta E_n| > |\delta E_t|$ (Figure 8b) does not significantly contribute to such transport, which may be observationally confirmed by a methodology developed by Izutsu et al. (2012). Thus, the mode with $|\delta E_n| > |\delta E_t|$ first needs to be converted through a parametric decay instability to the one with $|\delta E_n| \leq |\delta E_t|$ for massive transport to be realized (Lin et al., 2012). Besides such a nonlinear mode

conversion and likely ongoing Landau and transit damping of KAWs, whereby ions and electrons may be heated and undergo cross-field diffusion (Johnson & Cheng, 2001; Chaston et al., 2008; Moore et al., 2017; Wang et al., 2019), there may be a competition between possible amplification of KAWs via an inverse cascade (vortex merging) (Miura, 1997) and damping by the resistive ionosphere (Borovsky & Funsten, 2003) to which LLBL field lines are connected. These processes expected farther down the tail should be investigated in the future both observationally and numerically, in addition to the effects of eddy diffusion associated with flow velocity fluctuations (Matsumoto & Hoshino, 2004; Wang et al., 2010), in order to understand the formation process of the dense plasma sheet observed under northward IMF conditions (Wing et al., 2005).

6 Conclusions

We have investigated the generation process and mode properties of electromagnetic turbulence observed in KH vortices encountered at the dusk-flank magnetopause by the MMS spacecraft on 8 September 2015 under northward IMF conditions. The event on this day was compared with another MMS event under a similar solar wind and IMF condition in which magnetopause reconnection signatures but no KHI signatures were observed at the dayside magnetopause. We found that while high-latitude reconnection can excite a modest level of turbulence in the dayside low-latitude boundary layer, the KHI significantly enhances the turbulence level even in its early nonlinear phase, leading to magnetic energy spectra with power-law indices of about $-5/3$ at MHD scales and about $-8/3$ at sub-ion scales. Our wave vector and dispersion relation analysis assuming negligible displacement current (charge quasi-neutrality), plane waves/structures, and single mode for a given spacecraft frequency suggests that the turbulence consists of interlaced magnetic flux tubes of various scales (excluding electron scales) advected by plasma flows in the KH vortices, rather than of propagating normal mode waves. Combined with the evidence reported earlier for vortex induced reconnection (VIR) in the present MMS event (Eriksson et al., 2016; Li et al., 2016; Vernisse et al., 2016) and the results from 3D fully kinetic simulations that VIR in 3D can produce interlaced reconnected field lines, cause an efficient plasma mixing, and generate power-law magnetic energy spectra with a spectral index $-8/3$ at sub-ion scales (Nakamura, Hasegawa, et al., 2017; Nakamura, Eriksson, et al., 2017), we conclude that the sub-ion scale turbulence in the early nonlinear phase is not the primary cause of the plasma transport across the magnetopause, but a consequence of 3D VIR.

Acknowledgments

The MMS data used here are available from the MMS Science Data Center: <https://lasp.colorado.edu/mms/sdc/public/>. The analyses presented used version 3.3 of the FPI burst-mode data. Data access and processing was done using SPEDAS V3.1 (Angelopoulos et al., 2019). We thank Natalia Papitashvili at the National Space Science Data Center (NSSDC) of NASA/GSFC for the use of the OMNI 2 data set (OMNI data from <http://omniweb.gsfc.nasa.gov/>). For the simulation analyzed in this paper, we acknowledge PRACE for awarding us access to MareNostrum at Barcelona Supercomputing Center (BSC), Spain. An IDL code of the method to estimate the k -vectors used here is included in the Supporting Information of Bellan (2016), and a corresponding Matlab code is included in the

Supporting Information of the present paper. H.H. thanks Tony Lui, Yasuhito Narita, Luca Sorriso-Valvo, and Nobumitsu Yokoi for inspiring discussion.

References

- Ahirwar, G., Varma, P., & Tiwari, M. S. (2007). Beam effect on electromagnetic ion-cyclotron waves with general loss-cone distribution function in an anisotropic plasma-particle aspect analysis. *Ann. Geophys.*, 25, 557–568. <https://doi.org/10.5194/angeo-25-557-2007>
- Alexandrova, O., Lacombe, C., & Mangeney, A. (2008). Spectra and anisotropy of magnetic fluctuations in the Earth's magnetosheath: Cluster observations. *Ann. Geophys.*, 26, 3585–3596. <https://doi.org/10.5194/angeo-26-3585-2008>
- Alexandrova, O., Saur, J., Lacombe, C., Mangeney, A., Mitchell, J., Schwartz, S. J., & Robert, P. (2009). Universality of solar-wind turbulence spectrum from MHD to electron scales, *Phys. Rev. Lett.*, 103, 165003. <https://doi.org/10.1103/PhysRevLett.103.165003>
- Alexandrova, O., Chen, C. H. K., Sorriso-Valvo, L., Horbury, T. S., & Bale, S. D. (2013). Solar wind turbulence and the role of ion instabilities. *Space Sci. Rev.*, 178, 101–139. [doi:10.1007/s11214-013-0004-8](https://doi.org/10.1007/s11214-013-0004-8)
- Angelopoulos, V., Cruce, P., Drozdov, A., Grimes, E. W., et al. (2019). The Space Physics Environment Data Analysis System (SPEDAS). *Space Sci. Rev.*, 215, 9. <https://doi.org/10.1007/s11214-018-0576-4>
- Balbus, S. A., & Hawley, J. F. (1998). Instability, turbulence, and enhanced transport in accretion disks. *Rev. Modern Phys.*, 70, 1–53. <https://doi.org/10.1103/RevModPhys.70.1>
- Bellan, P. M. (2012). Improved basis set for low frequency plasma waves. *J. Geophys. Res.*, 117, A12219. [doi:10.1029/2012JA017856](https://doi.org/10.1029/2012JA017856)
- Bellan, P. M. (2016). Revised single-spacecraft method for determining wave vector k and resolving space-time ambiguity. *J. Geophys. Res. Space Physics*, 121, 8589–8599. [doi:10.1002/2016JA022827](https://doi.org/10.1002/2016JA022827)
- Borovsky, J. E., & Funsten, H. O. (2003). MHD turbulence in the Earth's plasma sheet: Dynamics, dissipation, and driving. *J. Geophys. Res.*, 108, 1284. [doi:10.1029/2002JA009625](https://doi.org/10.1029/2002JA009625)
- Borovsky, J. E. (2008). Flux tube texture of the solar wind: Strands of the magnetic carpet at 1 AU? *J. Geophys. Res.*, 113, A08110. [doi:10.1029/2007JA012684](https://doi.org/10.1029/2007JA012684)
- Bruno, R., & Carbone, V. (2013). The solar wind as a turbulence laboratory. *Living Rev. Solar Phys.*, 10, 2. [doi:10.12942/lrsp-2013-2](https://doi.org/10.12942/lrsp-2013-2)
- Burch, J. L., Moore, T. E., Torbert, R. B., & Giles, B. L. (2016). Magnetospheric Multiscale overview and science objectives. *Space Sci. Rev.*, 199, 5–21. [doi:10.1007/s11214-015-0164-9](https://doi.org/10.1007/s11214-015-0164-9)
- Chaston, C. C., Phan, T. D., Bonnell, J. W., Mozer, F. S., Acuna, M., Goldstein, M. L., Balogh, A., André, M., Rème, H., & Fazakerley, A. (2005). Drift-kinetic Alfvén waves observed near a reconnection X line in the Earth's magnetopause. *Phys. Rev. Lett.*, 95, 065002. <https://doi.org/10.1103/PhysRevLett.95.065002>

- Chaston, C. C., Wilber, M., Mozer, F. S., Fujimoto, M., Goldstein, M. L., Acuna, M., Rème, H., & Fazakerley, A. (2007). Mode conversion and anomalous transport in Kelvin-Helmholtz vortices and kinetic Alfvén waves at the Earth's magnetopause. *Phys. Rev. Lett.*, 99, 175004. <https://doi.org/10.1103/PhysRevLett.99.175004>
- Chaston, C., Bonnell, J., McFadden, J. P., et al. (2008). Turbulent heating and cross-field transport near the magnetopause from THEMIS. *Geophys. Res. Lett.*, 35, L17S08. doi:10.1029/2008GL033601
- Chen, C. H. K. (2016). Recent progress in astrophysical plasma turbulence from solar wind observations. *J. Plasma Phys.*, 82, 535820602. <https://doi.org/10.1017/S0022377816001124>
- Daughton, W., Nakamura, T. K. M., Karimabadi, H., Roytershteyn, V., & Loring, B. (2014). Computing the reconnection rate in turbulent kinetic layers by using electron mixing to identify topology. *Phys. Plasmas*, 21, 052307. doi:10.1063/1.4875730
- Di Mare, F., Sorriso-Valvo, L., Retinò, A., Malara, F., & Hasegawa, H. (2019). Evolution of turbulence in the Kelvin-Helmholtz instability in the terrestrial magnetopause. *Atmosphere*, 10(9), 561. <https://doi.org/10.3390/atmos10090561>
- Eastwood, J. P., Phan, T. D., Bale, S. D., & Tjulin, A. (2009). Observations of turbulence generated by magnetic reconnection. *Phys. Rev. Lett.*, 102, 035001. doi:10.1103/PhysRevLett.102.035001
- Ergun, R. E., Tucker, S., Westfall, J., et al. (2016). The axial double probe and fields signal processing for the MMS mission. *Space Sci. Rev.*, 199, 167–188. doi:10.1007/s11214-014-0115-x
- Eriksson, S., Hasegawa, H., Teh, W.-L., et al. (2009). Magnetic island formation between large-scale flow vortices at an undulating postnoon magnetopause for northward interplanetary magnetic field. *J. Geophys. Res.*, 114, A00C17. doi:10.1029/2008JA013505
- Eriksson, S., Lavraud, B., Wilder, F. D., et al. (2016). Magnetospheric Multiscale observations of magnetic reconnection associated with Kelvin-Helmholtz waves. *Geophys. Res. Lett.*, 43, 5606–5615. doi:10.1002/2016GL068783
- Fadanelli, S., Faganello, M., Califano, F., Cerri, S. S., Pegoraro, F., & Lavraud, B. (2018). North-south asymmetric Kelvin-Helmholtz instability and induced reconnection at the Earth's magnetospheric flanks. *Journal of Geophysical Research: Space Physics*, 123. <https://doi.org/10.1029/2018JA025626>
- Faganello, M., Califano, F., Pegoraro, F., & Andreussi, T. (2012). Double mid-latitude dynamical reconnection at the magnetopause: An efficient mechanism allowing solar wind to enter the Earth's magnetosphere. *Europhys. Lett.*, 100(6), 69001, doi:10.1209/0295-5075/100/69001
- Fox, N. J., Velli, M. C., Bale, S. D., Decker, R., Driesman, A., Howard, R. A., Kasper, J. C., Kinnison, J., Kusterer, M., Lario, D., Lockwood, M. K., McComas, D. J., Raouafi, N. E., & Szabo, A. (2016). The Solar Probe Plus mission: Humanity's first visit to our star. *Space Sci. Rev.*, 204, 7–48. <https://doi.org/10.1007/s11214-015-0211-6>

- Franci, L., Cerri, S. S., Califano, F., et al. (2017). Magnetic reconnection as a driver for a sub-ion-scale cascade in plasma turbulence. *Astrophys. J. Lett.*, 850, L16. doi:10.3847/2041-8213/aa93fb
- Fuselier, S. A. (1995). Kinetic aspects of reconnection at the magnetopause. in *Physics of the Magnetopause*, edited by P. Song, B. U. Ö. Sonnerup, and M. F. Thomsen, pp.181–187, AGU, Washington, D. C. doi 10.1029/GM090p0181
- Gaensler, B. M., Haverkorn, M., Burkhart, B., Newton-McGee, K. J., Ekers, R. D., Lazarian, A., McClure-Griffiths, N. M., Robishaw, T., Dickey, J. M., & Green, A. J. (2011). Low-Mach-number turbulence in interstellar gas revealed by radio polarization gradients. *Nature*, 478, 214–217. doi:10.1038/nature10446
- Gershman, D. J., F-Vinas, A., Dorelli, J. C., et al. (2017). Wave-particle energy exchange directly observed in a kinetic Alfvén-branch wave. *Nature Communications*, 8, 14719. doi:10.1038/ncomms14719
- Gershman, D. J., F.-Vinas, A., Dorelli, J. C., et al. (2018). Energy partitioning constraints at kinetic scales in low-beta turbulence. *Phys. Plasmas*, 25, 022303. <https://doi.org/10.1063/1.5009158>
- Goldreich, P., & Sridhar, S. (1995). Toward a theory of interstellar turbulence. 2: Strong Alfvénic turbulence. *Astrophys. J.*, 438, 763–775. doi:10.1086/175121
- Hasegawa, A. (1976). Particle acceleration by MHD surface wave and formation of aurora. *J. Geophys. Res.*, 81, 5083–5090. doi:10.1029/JA081i028p05083
- Hasegawa, H. (2012). Structure and dynamics of the magnetopause and its boundary layers. *Monogr. Environ. Earth Planets*, 1(2), 71–119, doi:10.5047/meep.2012.00102.0071
- Hasegawa, H., Fujimoto, M., Phan, T.-D., Rème, H., Balogh, A., Dunlop, M. W., ... TanDokoro, R. (2004). Transport of solar wind into Earth’s magnetosphere through rolled-up Kelvin–Helmholtz vortices. *Nature*, 430, 755–758. <https://doi.org/10.1038/nature02799>
- Hasegawa, H., Fujimoto, M., Takagi, K., Saito, Y., Mukai, T., & Rème, H. (2006). Single-spacecraft detection of rolled-up Kelvin-Helmholtz vortices at the flank magnetopause. *J. Geophys. Res.*, 111, A09203. doi:10.1029/2006JA011728
- Hasegawa, H., McFadden, J. P., Constantinescu, O. D., et al. (2009). Boundary layer plasma flows from high-latitude reconnection in the summer hemisphere for northward IMF: THEMIS multi-point observations. *Geophys. Res. Lett.*, 36, L15107. doi:10.1029/2009GL039410
- Hasegawa, H., Retinò, A., Vaivads, A., Khotyaintsev, Y., André, M., Nakamura, T. K. M., Teh, W.-L., Sonnerup, B. U. Ö., Schwartz, S. J., Seki, Y., Fujimoto, M., Saito, Y., Rème, H., & Canu, P. (2009). Kelvin-Helmholtz waves at the Earth’s magnetopause: Multiscale development and associated reconnection. *J. Geophys. Res.*, 114, A12207. doi:10.1029/2009JA014042
- Haw, M. A., Seo, B., & Bellan, P. M. (2019). Laboratory measurement of large-amplitude whistler pulses generated by fast magnetic reconnection. *Geophysical Research Letters*, 46, 7105–7112. <https://doi.org/10.1029/2019GL082621>

- Hollweg, J. V. (1999). Kinetic Alfvén wave revisited. *J. Geophys. Res.*, 104(A7), 14811–14819. doi:10.1029/1998JA900132
- Hu, Q., Zheng, J., Chen, Y., le Roux, J., & Zhao, L. (2018). Automated Detection of Small-scale Magnetic Flux Ropes in the Solar Wind: First Results from the Wind Spacecraft Measurements, *Astrophysical Journal Supplement Series*, 239, 12. <https://doi.org/10.3847/1538-4365/aae57d>
- Izutsu, T., Hasegawa, H., Nakamura, T. K. M., & Fujimoto, M. (2012) Plasma transport induced by kinetic Alfvén wave turbulence. *Phys. Plasmas*, 19, 102305. doi:10.1063/1.4759167
- Johnson, J. R., & Cheng, C. Z. (1997). Kinetic Alfvén waves and plasma transport at the magnetopause. *Geophys. Res. Lett.*, 24, 1423–1426. <https://doi.org/10.1029/97GL01333>
- Johnson, J. R., Cheng, C. Z., & Song, P. (2001). Signatures of mode conversion and kinetic Alfvén waves at the magnetopause. *Geophys. Res. Lett.*, 28(2), 227–230. <https://doi.org/10.1029/2000GL012048>
- Johnson, J. R., & Cheng, C. Z. (2001). Stochastic ion heating at the magnetopause due to kinetic Alfvén waves. *Geophys. Res. Lett.*, 28, 4421–4424. <https://doi.org/10.1029/2001GL013509>
- Karimabadi, H., Roytershteyn, V., Vu, H. X., et al. (2014). The link between shocks, turbulence, and magnetic reconnection in collisionless plasmas. *Phys. Plasmas*, 21, 062308. doi:10.1063/1.4882875
- Kavosi, S., & Raeder, J. (2015). Ubiquity of Kelvin-Helmholtz waves at Earth’s magnetopause. *Nature Commun.*, 6, 7019. doi:10.1038/ncomms8019
- Lavraud, B., Thomsen, M. F., Lefebvre, B., Schwartz, S. J., Seki, K., Phan, T. D., Wang, Y. L., Fazakerley, A., Rème, H., & Balogh, A. (2006). Evidence for newly closed magnetosheath field lines at the dayside magnetopause under northward IMF. *J. Geophys. Res.*, 111, A05211. doi:10.1029/2005JA011266
- Li, W., André, M., Khotyaintsev, Yu. V., et al. (2016). Kinetic evidence of magnetic reconnection due to Kelvin-Helmholtz waves. *Geophys. Res. Lett.*, 43, 5635–5643. doi:10.1002/2016GL069192
- Lin, D., Wang, C., Li, W., Tang, B., Guo, X., & Peng, Z. (2014). Properties of Kelvin-Helmholtz waves at the magnetopause under northward interplanetary magnetic field: Statistical study, *J. Geophys. Res. Space Physics*, 119, 7485–7494, doi:10.1002/2014JA020379
- Lin, Y., Johnson, J. R., & Wang, X. Y. (2010). Hybrid simulation of mode conversion at the magnetopause. *J. Geophys. Res.*, 115, A04208. doi:10.1029/2009JA014524
- Lin, Y., Johnson, J. R., & Wang, X. Y. (2012). Three-dimensional mode conversion associated with kinetic Alfvén waves. *Phys. Rev. Lett.*, 109, 125003. doi:10.1103/PhysRevLett.109.125003
- Lindqvist, P.-A., Olsson, G., Torbert, R. B., King, B., Granoff, M., et al. (2016). The Spin-plane Double Probe electric field instrument for MMS. *Space Sci. Rev.*, 199, 137–165. doi:10.1007/s11214-014-0116-9

- Matsumoto, Y., & Hoshino, M. (2004). Onset of turbulence induced by a Kelvin-Helmholtz vortex. *Geophys. Res. Lett.*, 31, L02807. doi:10.1029/2003GL018195
- Matthaeus, W. H., Wan, M., Servidio, S., Greco, A., Osman, K. T., Oughton, S., & Dmitruk, P. (2015). Intermittency, nonlinear dynamics and dissipation in the solar wind and astrophysical plasmas. *Phil. Trans. R. Soc. A*, 373, 20140154. <https://doi.org/10.1098/rsta.2014.0154>
- Miesch, M. S., Elliott, J. R., Toomre, J., Clune, T. L., Glatzmaier, G. A., & Gilman, P. A. (2000). Three-dimensional spherical simulations of solar convection. I. Differential rotation and pattern evolution achieved with laminar and turbulent states. *Astrophys. J.*, 532, 593–615. <https://doi.org/10.1086/308555>
- Miura, A. (1997). Compressible magnetohydrodynamic Kelvin-Helmholtz instability with vortex pairing in the two-dimensional transverse configuration. *Phys. Plasmas*, 4, 2871–2885. <https://doi.org/10.1063/1.872419>
- Moore, T. W., Nykyri, K., & Dimmock, A. P. (2016). Cross-scale energy transport in space plasmas. *Nature Phys.*, 12, 1164–1169. doi:10.1038/nphys3869
- Moore, T. W., Nykyri, K., & Dimmock, A. P. (2017). Ion-scale wave properties and enhanced ion heating across the low-latitude boundary layer during Kelvin-Helmholtz instability. *Journal of Geophysical Research: Space Physics*, 122, 11,128–11,153. <https://doi.org/10.1002/2017JA024591>
- Nakamura, T. K. M. (2020). The Earth’s low-latitude boundary layer, in *Magnetospheres in the Solar System* (eds. R Maggiolo, N. Andre, H. Hasegawa, & D. Welling), John Wiley & Sons, Inc, Hoboken, NJ.
- Nakamura, T. K. M., Fujimoto, M., & Otto, A. (2006). Magnetic reconnection induced by weak Kelvin-Helmholtz instability and the formation of the low-latitude boundary layer. *Geophys. Res. Lett.*, 33, L14106. doi:10.1029/2006GL026318
- Nakamura, T. K. M., Hasegawa, H., Shinohara, I., & Fujimoto, M. (2011). Evolution of an MHD-scale Kelvin-Helmholtz vortex accompanied by magnetic reconnection: Two-dimensional particle simulations. *J. Geophys. Res.*, 116, A03227. doi:10.1029/2010JA016046
- Nakamura, T. K. M., Daughton, W., Karimabadi, H., & Eriksson, S. (2013). Three-dimensional dynamics of vortex-induced reconnection and comparison with THEMIS observations. *J. Geophys. Res. Space Physics*, 118, 5742–5757. doi:10.1002/jgra.50547
- Nakamura, T. K. M., Hasegawa, H., Daughton, W., Eriksson, S., Li, W. Y., & Nakamura, R. (2017). Turbulent mass transfer caused by vortex induced reconnection in collisionless magnetospheric plasmas. *Nature Communications*, 8, 1582. doi:10.1038/s41467-017-01579-0
- Nakamura, T. K. M., Eriksson, S., Hasegawa, H., Zenitani, S., Li, W. Y., Genestreti, K. J., Nakamura, R., & Daughton, W. (2017). Mass and energy transfer across the Earth’s magnetopause caused by vortex-induced reconnection. *Journal of Geophysical Research: Space Physics*, 122, 11505–11522, <https://doi.org/10.1002/2017JA024346>

- Nakamura, T. K. M., Stawarz, J. E., Hasegawa, H., Narita, Y., Franci, L., Wilder, F. D., Nakamura, R., & Nystrom, W. D. (2019). Effects of fluctuating magnetic field on the growth of the Kelvin-Helmholtz instability at the Earth's magnetopause. Preprint on <https://essoar.org> (2019). <https://doi.org/10.1002/essoar.10501061.1>
- Narita, Y., Gary, S. P., Saito, S., Glassmeier, K.-H., & Motschmann, U. (2011). Dispersion relation analysis of solar wind turbulence. *Geophys. Res. Lett.*, 38, L05101. doi:10.1029/2010GL046588
- Narita, Y., Plaschke, F., Nakamura, R., et al. (2016). Wave telescope technique for MMS magnetometer. *Geophys. Res. Lett.*, 43, 4774–4780. doi:10.1002/2016GL069035
- Narita, Y., Nakamura, R., Baumjohann, W., et al. (2016). On electron-scale whistler turbulence in the solar wind, *Astrophys. J. Lett.*, 827, L8, doi:10.3847/2041-8205/827/1/L8
- Neubauer, F. M., & Glassmeier, K.-H. (1990). Use of an array of satellites as a wave telescope, *J. Geophys. Res.*, 95, 19115–19122. <https://doi.org/10.1029/JA095iA11p19115>
- Nishino, M. N., Fujimoto, M., Ueno, G., Mukai, T., & Saito, Y. (2007). Origin of temperature anisotropies in the cold plasma sheet: Geotail observations around the Kelvin-Helmholtz vortices. *Ann. Geophys.*, 25, 2069–2086. <https://doi.org/10.5194/angeo-25-2069-2007>.
- Nykyri, K., & Otto, A. (2001). Plasma transport at the magnetospheric boundary due to reconnection in Kelvin-Helmholtz vortices. *Geophys. Res. Lett.*, 28, 3565–3568. <https://doi.org/10.1029/2001GL013239>
- Nykyri, K., Grison, B., Cargill, P. J., Lavraud, B., Lucek, E., Dandouras, I., Balogh, A., Cornilleau-Wehrlin, N., and Reme, H. (2006). Origin of the turbulent spectra in the high-altitude cusp: Cluster spacecraft observations. *Ann. Geophys.*, 24, 1057–1075. <https://doi.org/10.5194/angeo-24-1057-2006>
- Nykyri, K., Ma, X., Dimmock, A., Foullon, C., Otto, A., & Osmane, A. (2017). Influence of velocity fluctuations on the Kelvin-Helmholtz instability and its associated mass transport. *J. Geophys. Res. Space Physics*, 122, 9489–9512. doi:10.1002/2017JA024374
- Øieroset, M., Phan, T. D., Angelopoulos, V., Eastwood, J. P., McFadden, J., Larson, D., ... Raeder, J. (2008). THEMIS multi-spacecraft observations of magnetosheath plasma penetration deep into the dayside low-latitude magnetosphere for northward and strong by IMF. *Geophys. Res. Lett.*, 35, L17S11. <https://doi.org/10.1029/2008GL033661>
- Paschmann, G., Baumjohann, W., Sckopke, N., Phan, T.-D., and Lühr, H. (1993). Structure of the dayside magnetopause for low magnetic shear. *J. Geophys. Res.*, 98(A8), 13409–13422. doi:10.1029/93JA00646
- Phan, T. D., Eastwood, J. P., Shay, M. A., Drake, J. F., Sonnerup, B. U. Ö., et al. (2018). Electron magnetic reconnection without ion coupling in Earth's turbulent magnetosheath. *Nature*, 557, 202–206. doi:10.1038/s41586-018-0091-5
- Pinçon, J. L., and Lefeuvre, F. (1991). Local characterization of homogeneous turbulence in a space plasma from simultaneous Measurements of field components at several points in space. *J. Geophys. Res.*, 96(A2), 1789–1802. doi:10.1029/90JA02183
- Pollock, C., Moore, T., Jacques, A., et al. (2016). Fast Plasma Investigation for Magnetospheric Multiscale. *Space Sci. Rev.*, 199, 331–406. doi:10.1007/s11214-016-0245-4

- Rezeau, L., & Belmont, G. (2001). Magnetic turbulence at the magnetopause, A key problem for understanding the solar wind/magnetosphere exchanges. *Space Sci. Rev.*, 95, 427–441. <https://doi.org/10.1023/A:1005273124854>
- Russell, C. T., Anderson, B. J., Baumjohann, W., et al. (2016). The Magnetospheric Multiscale Magnetometers. *Space Sci. Rev.*, 199, 189–256. doi:10.1007/s11214-014-0057-3
- Sahraoui, F., Belmont, G., Rezeau, L., Cornilleau-Wehrin, N., Pincon, J. L., & Balogh, A. (2006). Anisotropic turbulent spectra in the terrestrial magnetosheath as seen by the Cluster spacecraft. *Phys. Rev. Lett.*, 96, 075002. <https://doi.org/10.1103/PhysRevLett.96.075002>
- Sahraoui, F., Goldstein, M. L., Robert, P., & Khotyaintsev, Y. V. (2009). Evidence of a cascade and dissipation of solar-wind turbulence at the electrons gyroscale. *Phys. Rev. Lett.*, 102, 231102. doi:10.1103/PhysRevLett.102.231102
- Sahraoui, F., Goldstein, M. L., Belmont, G., Canu, P., & Rezeau, L. (2010). Three dimensional anisotropic k spectra of turbulence at subproton scales in the solar wind. *Phys. Rev. Lett.*, 105(13), 131101. doi:10.1103/PhysRevLett.105.131101
- Smyth, W. D., & Moum, J. N. (2012). Ocean mixing by Kelvin-Helmholtz instability. *Oceanography*, 25(2), 140–149. <https://doi.org/10.5670/oceanog.2012.49>
- Song, P., & Russell, C. T. (1992). Model of the formation of the low-latitude boundary layer for strongly northward interplanetary magnetic field. *J. Geophys. Res.*, 97(A2), 1411–1420. <https://doi.org/10.1029/91JA02377>
- Soucek, J., Escoubet, C. P., & Grison, B. (2015). Magnetosheath plasma stability and ULF wave occurrence as a function of location in the magnetosheath and upstream bow shock parameters. *J. Geophys. Res. Space Physics*, 120, 2838–2850. doi:10.1002/2015JA021087
- Stawarz, J. E., Eriksson, S., Wilder, F. D., et al. (2016). Observations of turbulence in a Kelvin-Helmholtz event on 8 September 2015 by the Magnetospheric Multiscale mission. *J. Geophys. Res. Space Physics*, 121, 11,021–11,034. doi:10.1002/2016JA023458
- Sturner, A. P., Eriksson, S., Nakamura, T., Gershman, D. J., Plaschke, F., Ergun, R. E., et al. (2018). On multiple Hall-like electron currents and tripolar guide magnetic field perturbations during Kelvin-Helmholtz waves. *Journal of Geophysical Research: Space Physics*. 123, 1305–1324. <https://doi.org/10.1002/2017JA024155>
- Vasavada, A. R., & Showman, A. P. (2005). Jovian atmospheric dynamics: an update after Galileo and Cassini. *Rep. Prog. Phys.*, 68, 1935. <https://doi.org/10.1088/0034-4885/68/8/R06>
- Vernisse, Y., Lavraud, B., Eriksson, S., et al. (2016). Signatures of complex magnetic topologies from multiple reconnection sites induced by Kelvin-Helmholtz instability. *J. Geophys. Res. Space Physics*, 121, 9926–9939. doi:10.1002/2016JA023051
- Wang, C.-P., Lyons, L. R., Nagai, T., Weygand, J. M., & Lui, A. T. Y. (2010). Evolution of plasma sheet particle content under different interplanetary magnetic field conditions. *J. Geophys. Res.*, 115, A06210. doi:10.1029/2009JA015028

- 876 Wang, C.-P., Fuselier, S. A., Hairston, M., Zhang, X.-j., Zou, S., Avanov, L. A., et al. (2019).
877 Event studies of O⁺ density variability within quiet-time plasma sheet. *Journal of*
878 *Geophysical Research: Space Physics*, 124, 4168–4187.
879 <https://doi.org/10.1029/2019JA026644>
- 880 Wing, S., Johnson, J. R., Newell, P. T., & Meng, C.-I. (2005). Dawn-dusk asymmetries, ion
881 spectra, and sources in the northward interplanetary magnetic field plasma sheet. *J.*
882 *Geophys. Res.*, 110, A08205. doi:10.1029/2005JA011086
- 883 Wilder, F. D., Ergun, R. E., Schwartz, S. J., et al. (2016). Observations of large-amplitude,
884 parallel, electrostatic waves associated with the Kelvin-Helmholtz instability by the
885 Magnetospheric Multiscale mission. *Geophys. Res. Lett.*, 43, 8859–8866.
886 doi:10.1002/2016GL070404
- 887 Wyngaard, J. C. (1992). Atmospheric turbulence. *Annu. Rev. Fluid Mech.*, 24, 205-234.
888 <https://doi.org/10.1146/annurev.fl.24.010192.001225>
- 889 Zimbardo, G., Greco, A., Sorriso-Valvo, L., et al. (2010). Magnetic turbulence in the geospace
890 environment. *Space Sci. Rev.*, 156, 89–134. doi:10.1007/s11214-010-9692-5
891

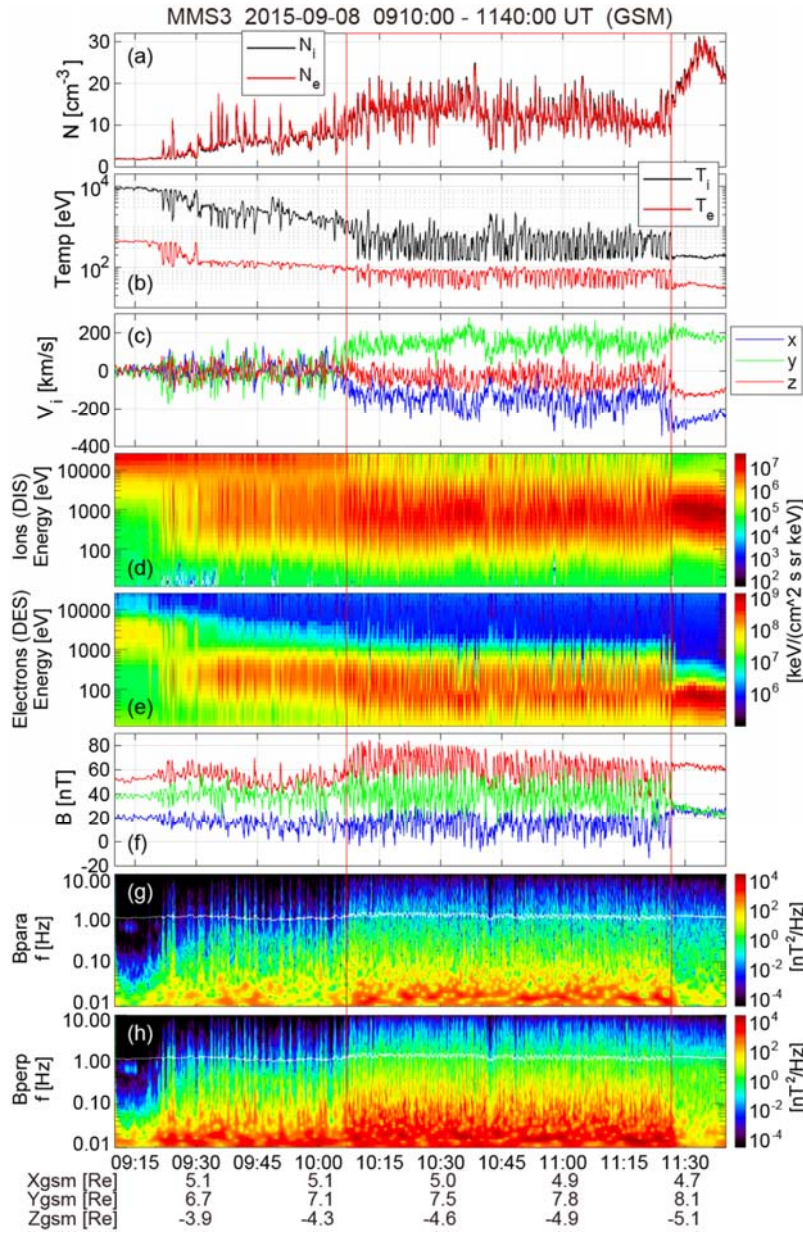


Figure 1. MMS3 fast survey-mode observations of Kelvin-Helmholtz (KH) waves at the postnoon magnetopause on 8 September 2015 for the interval 0910–1140 UT. (a) Ion and electron densities, (b) ion and electron temperatures assuming isotropic velocity distributions, (c) three GSM components of the ion velocity, (d,e) energy versus time spectrograms of omnidirectional ions and electrons from the dual ion spectrometer (DIS) and dual electron spectrometer (DES) parts, respectively, of the fast plasma investigation (FPI) instrument suite, (f) GSM components of the magnetic field, and (g,h) Wavelet power spectra of the magnetic field fluctuations parallel and perpendicular to the mean field, with the proton cyclotron frequency marked by the white curve. The KH-active interval 1007–1127 UT between the two vertical red lines is used to derive turbulent spectra in Figure 2.

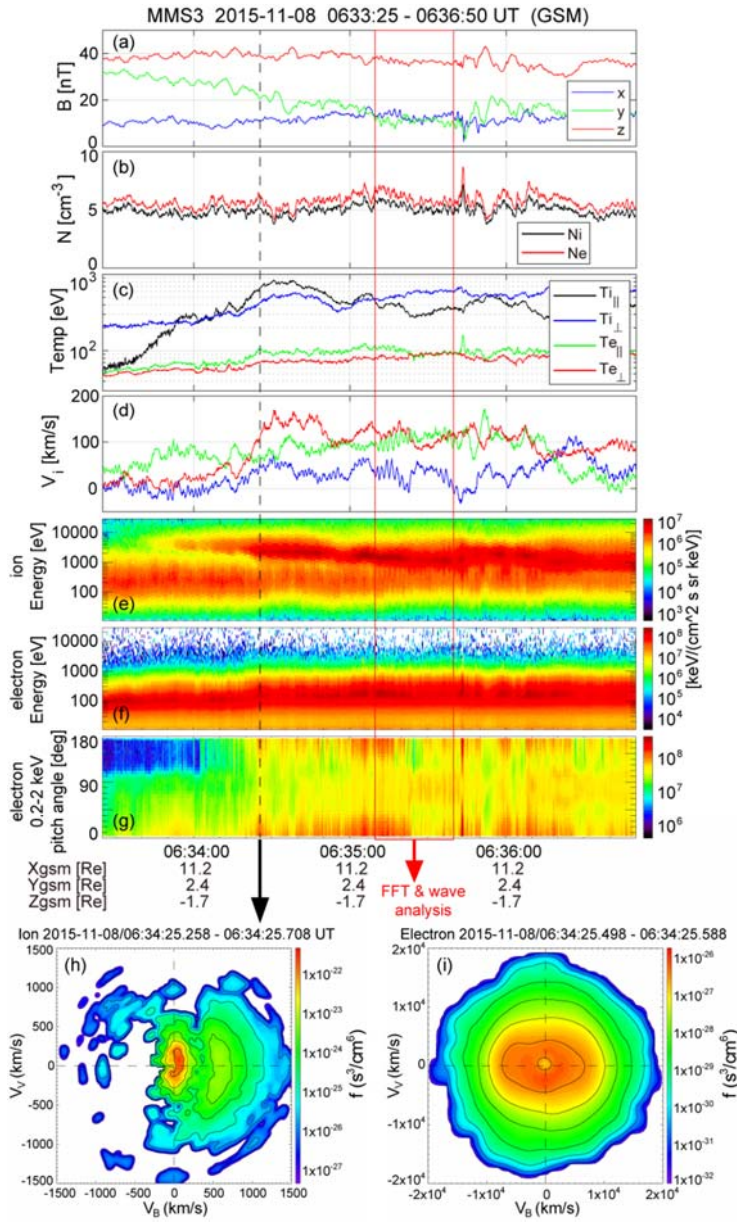


Figure 2. MMS3 burst-mode observations of a dayside, equatorial magnetopause crossing under dominantly northward IMF on 8 November 2015, 0633:25–0636:50 UT. (a) GSM components of the magnetic field, (b) ion and electron densities, (c) ion and electron temperatures in the directions parallel and perpendicular to the magnetic field, (d) GSM components of the ion velocity, (e,f) energy-time spectrograms of omnidirectional ions and electrons, (g) pitch-angle distributions of 0.2–2 keV electrons, and (h,i) two-dimensional cuts of ion and electron velocity distributions by the plane containing the magnetic field and velocity vectors at the time marked by the vertical dashed line. The 30-sec interval enclosed by the red box is used for the spectral and k-vector analyses as shown in Figures 3, 6, and 7.

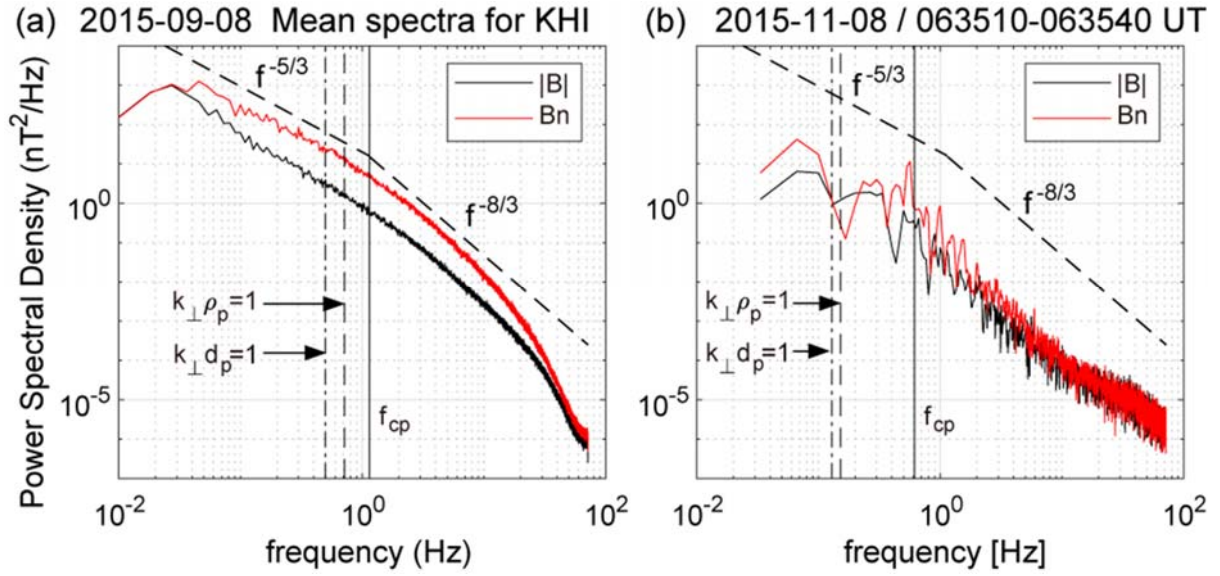


Figure 3. (a) Average power spectra of the magnetic field intensity and field component perpendicular to the mean field and roughly normal to the nominal magnetopause for magnetosphere-side intervals of the KH-active period 1007–1127 UT in Figure 1. (b) Power spectra for the magnetopause boundary layer interval in Figure 2. Proton cyclotron frequency f_{cp} , $k_{\perp}\rho_p = 1$, and $k_{\perp}d_p = 1$ are shown assuming that the observed frequency spectra are equivalent to the wave number spectra in the perpendicular direction and the Taylor hypothesis $\omega_{sc} = 2\pi f_{sc} = \mathbf{k}_{\perp} \cdot \langle \mathbf{v}_{i\perp} \rangle$ is satisfied, where ρ_p is proton gyroradius, d_p is proton inertial length, and $\langle \mathbf{v}_{i\perp} \rangle$ is the perpendicular component of the ion bulk velocity.

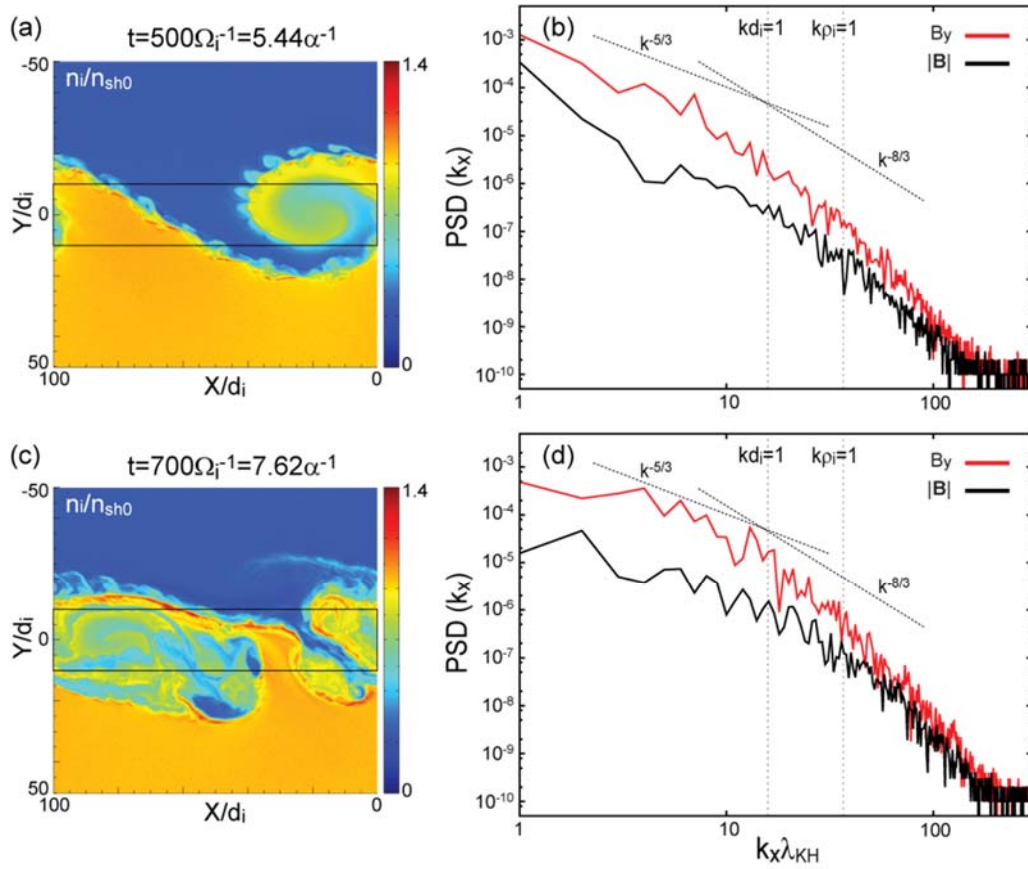


Figure 4. (a,c) Density profiles in the XY plane at $t = 500\Omega_i^{-1}$ and $t = 700\Omega_i^{-1}$ from a 3D kinetic simulation of the KHI (Nakamura, 2020, where $\Omega_i = eB_0/m_i$ and $\alpha = V_0/\lambda_{KHI}$, the total velocity jump across the initial shear layer divided by the most unstable KHI wavelength. The X axis is roughly antiparallel to the initial magnetosheath flow, and the Y axis is normal to the initial velocity shear and current layers. The average wave number spectra of the magnetic energy density in normalized unit (b,d) are computed by use of the simulation data in the domain enclosed by the black boxes.

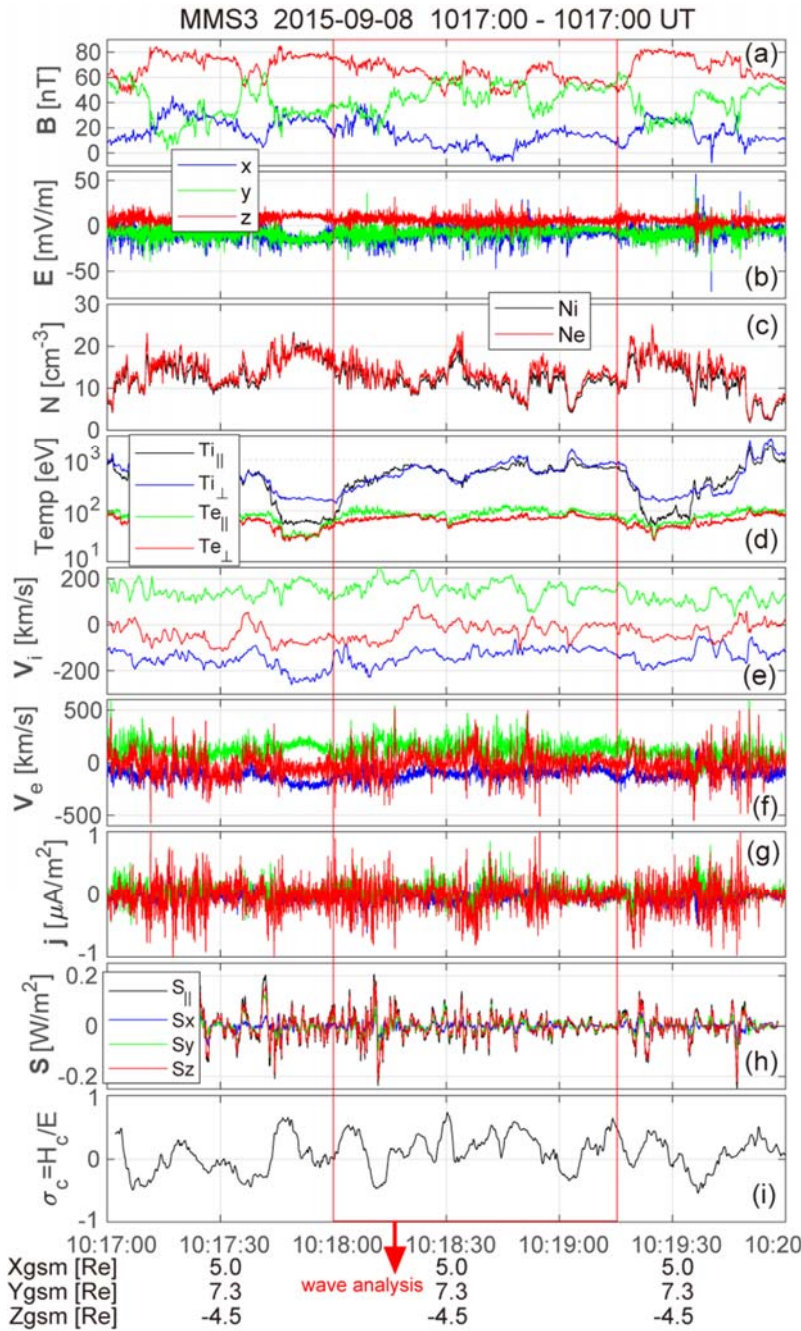


Figure 5. An example of the KH-active boundary layer intervals on 8 September 2015 used for the k-vector analysis. (a,b) GSM components of the magnetic and electric fields, (c) ion and electron densities, (d) ion and electron temperatures in both the parallel and perpendicular directions, (e,f) ion and electron velocities, and (g) current density based on the FPI measurements, (h) parallel and GSM components of Poynting flux, $\mathbf{S} = \delta\mathbf{E} \times \delta\mathbf{B}/\mu_0$, and (i) normalized ion cross helicities, $\sigma_c = H_c/E$, the ratio between the cross helicity and average energy (see text for details), all from the MMS3 spacecraft. The magnetosphere-side interval enclosed by the red box is used in the k-vector analysis.

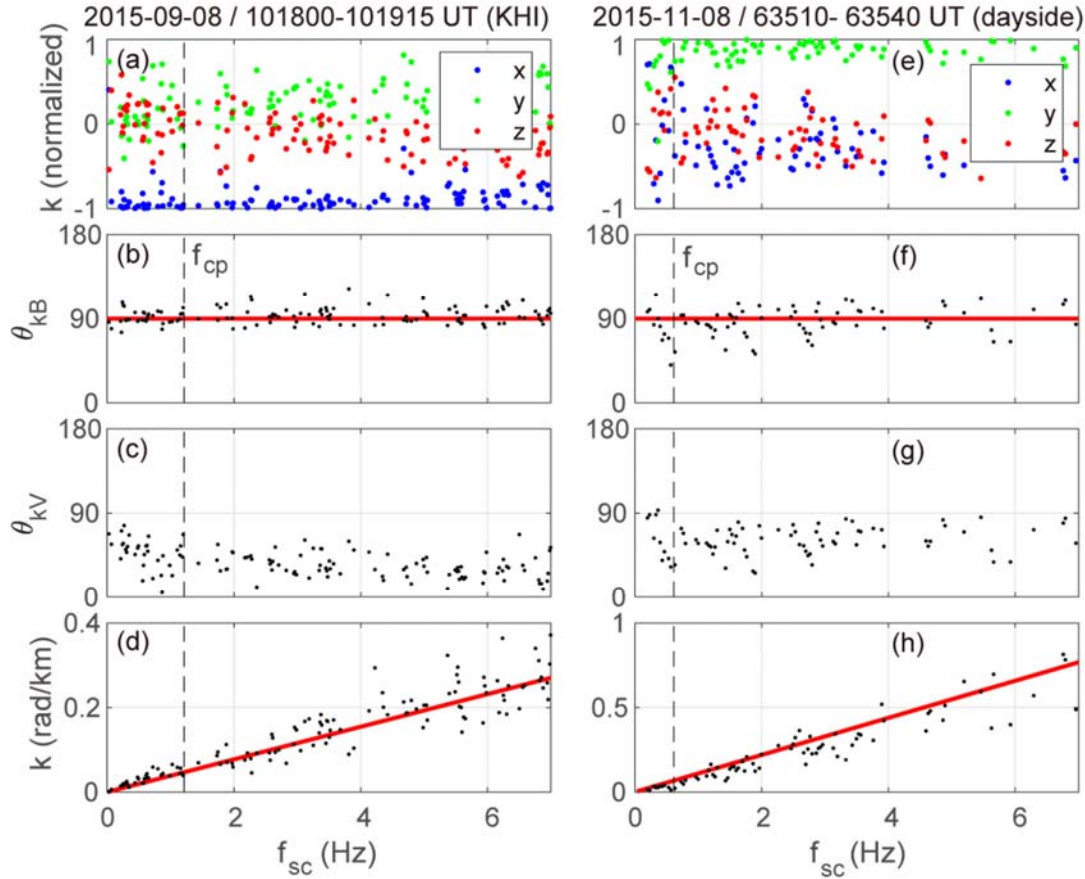


Figure 6. Wave vector properties derived from Bellan's method for the KH-active boundary layer interval (left: 1018:00–1019:15 UT) and dayside reconnection jet interval (right: 0635:10–0635:40 UT). (a,e) GSM components of the orientations of the k -vectors, (b,f) angles between the k -vectors and the mean magnetic field direction, (c,g) angles between the k -vectors and the mean ion flow direction, and (d,h) the magnitude of the wave number, as a function of frequency f_{sc} in the spacecraft frame. The red line in panels (d,h) shows the Taylor condition $2\pi f_{sc} = k \langle v_i \rangle \cos \langle \theta_{kv} \rangle$, where $\langle v_i \rangle$ is the mean ion speed for the analysis interval and $\langle \theta_{kv} \rangle$ is the average angle between the k -vectors and $\langle \mathbf{v}_i \rangle$.

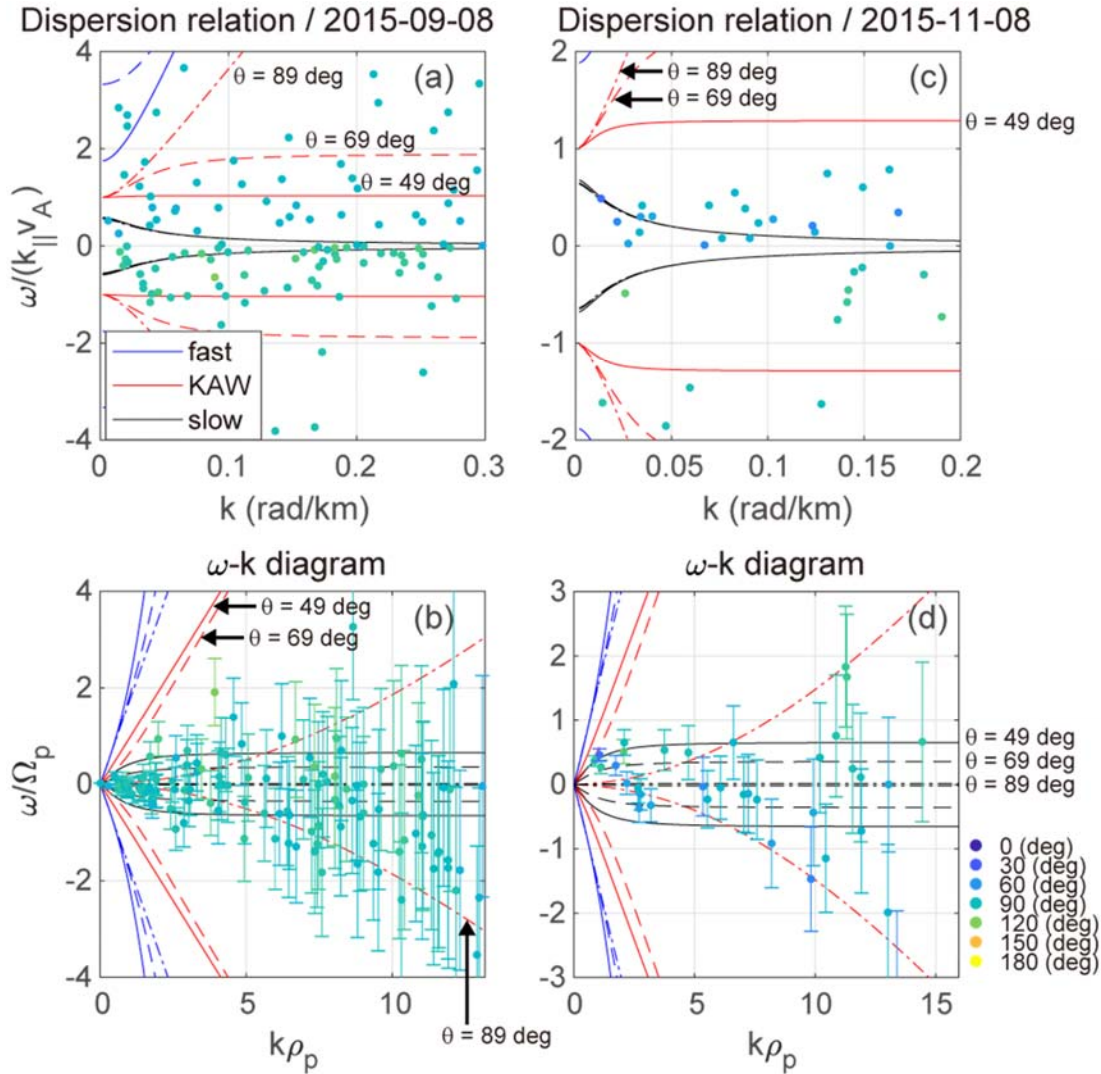


Figure 7. Dispersion relations derived from Bellan's method in which the Doppler effect is subtracted for the KHI (left) and dayside reconnection (right) events. (a,c) Parallel phase velocity $\omega_{pl}/(k_{\parallel}v_A)$ normalized to the Alfvén speed versus wave number, and (b,d) ω_{pl} - k diagrams normalized to proton cyclotron frequency and proton gyroradius, respectively. Colors of the points denote the orientations of the k -vectors with respect to the magnetic field. Theoretical linear dispersion relations for the fast (blue), intermediate (red), and slow (black) modes are derived from equation (29) in Bellan (2012) based on the two-fluid model. Dispersion curves for three propagation angles $\theta = 49^\circ$ (solid), 69° (dashed), and 89° (dash-dot) with respect to the magnetic field are shown here. Error bars in panels (b,d) correspond to the standard deviation σ_v of the ion flow velocity component along \mathbf{k} for the analysis interval, i.e., $k\sigma_v$.

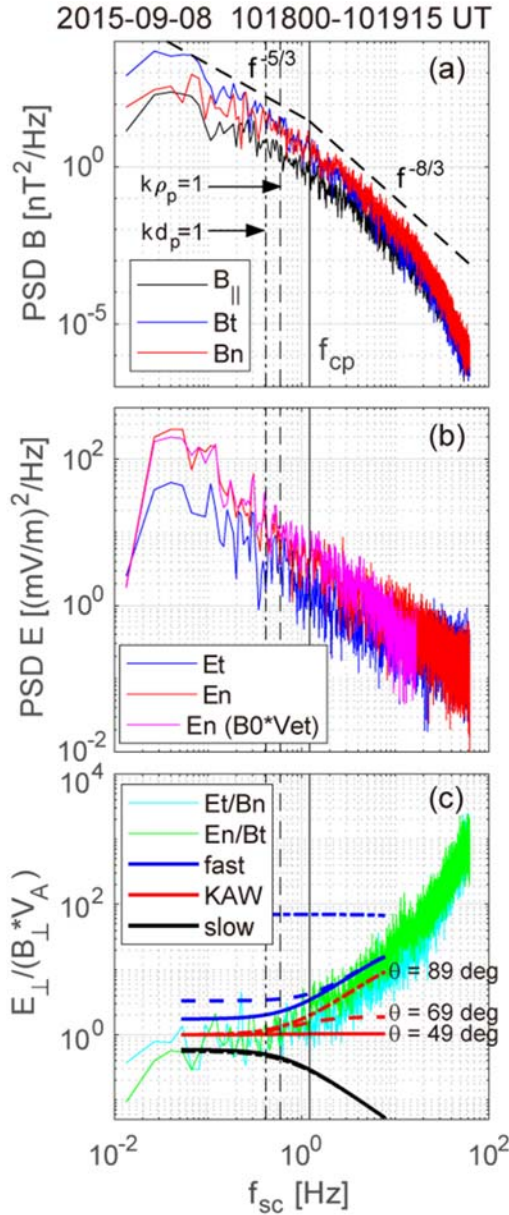


Figure 8. (a) Power spectra of the magnetic field components parallel and perpendicular to the mean magnetic field. The perpendicular components δB_n and δB_t are roughly normal and tangential, respectively, to the magnetopause. (b) Power spectra of the electric field components δE_n and δE_t perpendicular to the mean magnetic field in the mean flow frame. The magenta line shows the spectrum of the normal component of the convection electric field $\mathbf{E}_c = -\mathbf{v}_{e\perp} \times \mathbf{B}_0$. (c) $\delta E_t/\delta B_n$ (cyan) and $\delta E_n/\delta B_t$ (green), normalized to the Alfvén speed. The curves show linear dispersion relations based on the two-fluid model (Bellan, 2012) of fast, intermediate (KAW), and slow mode waves for three propagation angles $\theta = 49^\circ$ (solid), 69° (dashed), and 89° (dash-dot) with respect to the background magnetic field.

Generation of Turbulence in Kelvin-Helmholtz Vortices at the Earth's Magnetopause: Magnetospheric Multiscale Observations

H. Hasegawa¹, T. K. M. Nakamura², D. J. Gershman³, Y. Nariyuki⁴, A. F.-Viñas³, B. L. Giles³, B. Lavraud⁵, C. T. Russell⁶, Y. V. Khotyaintsev⁷, R. E. Ergun⁸, and Y. Saito¹

¹Institute of Space and Astronautical Science, Japan Aerospace Exploration Agency, Sagami-hara, Japan.

²Space Research Institute, Austrian Academy of Sciences, Graz, Austria.

³NASA Goddard Space Flight Center, Greenbelt, MD, USA.

⁴Faculty of Human Development, University of Toyama, Toyama, Japan.

⁵Institut de Recherche en Astrophysique et Planétologie, CNRS, UPS, CNES, Université de Toulouse, Toulouse, France.

⁶Department of Earth, Planetary, and Space Sciences, University of California, Los Angeles, California, USA.

⁷Swedish Institute of Space Physics, Uppsala, Sweden.

⁸Department of Astrophysical and Planetary Sciences, University of Colorado, Boulder, Colorado, USA.

Contents of this file

Figures S1 to S5
Table S1

Additional Supporting Information (File uploaded separately)

The second Supporting Information contains a Matlab code for the single-spacecraft method to estimate wave vectors, translated from the IDL version developed by Bellan (2016).

Introduction

The supporting information includes solar wind and interplanetary magnetic field conditions surrounding the two MMS events studied in the paper (Figures S1 and S2). It also contains results (Figures S3-S5) from Bellan's single-spacecraft method to estimate wave vectors (Bellan, 2016) applied to synthetic magnetic field and current density data taken by a virtual spacecraft passing through a simulated three-dimensional Kelvin-Helmholtz (KH) vortex, as reported by Nakamura (2020).

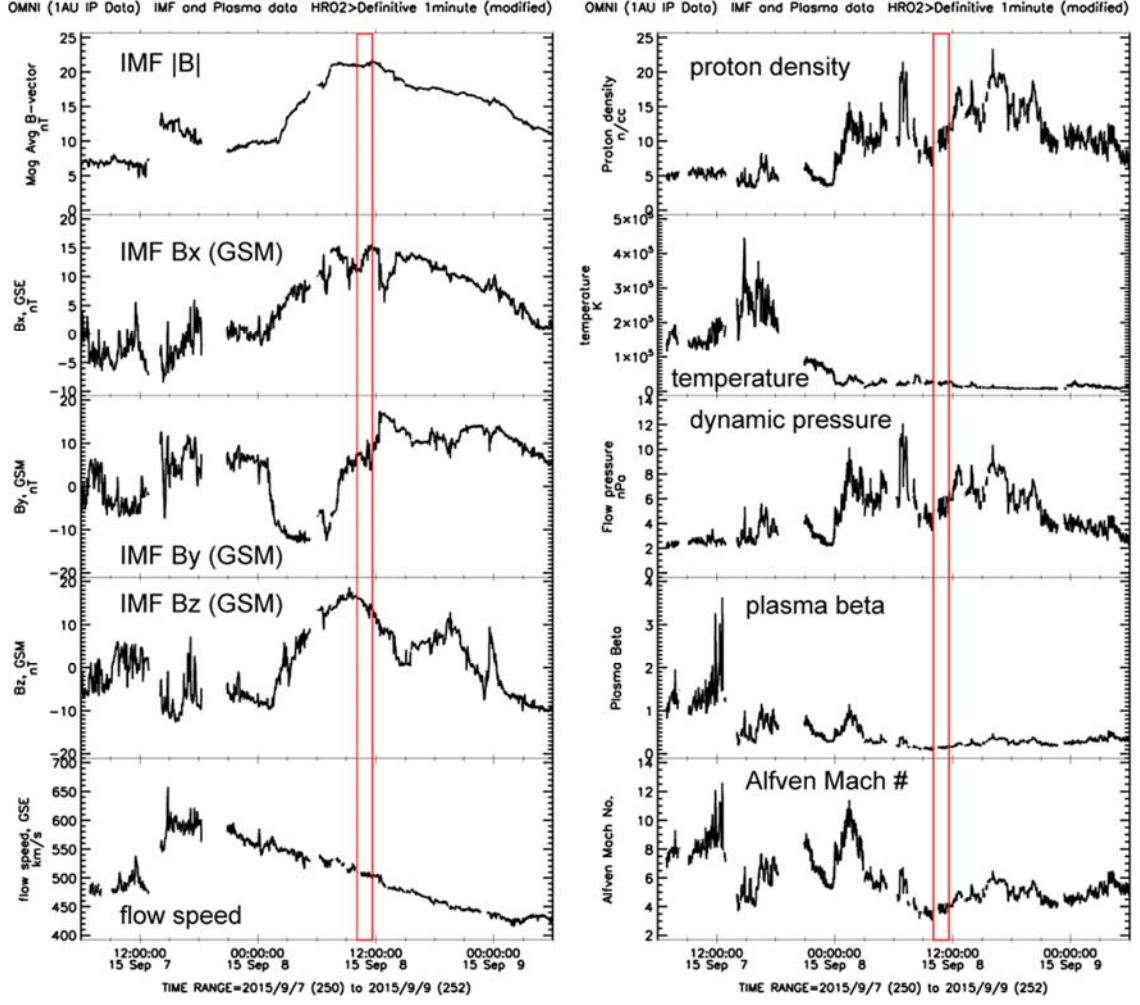


Figure S1. Solar wind and IMF conditions based on the OMNI database over a 2-day period from 2015-09-07, 0600 UT to 2015-09-09, 0600 UT, surrounding the MMS KHI+RX event on 2015-09-08. The red box marks the time interval studied in the main text.

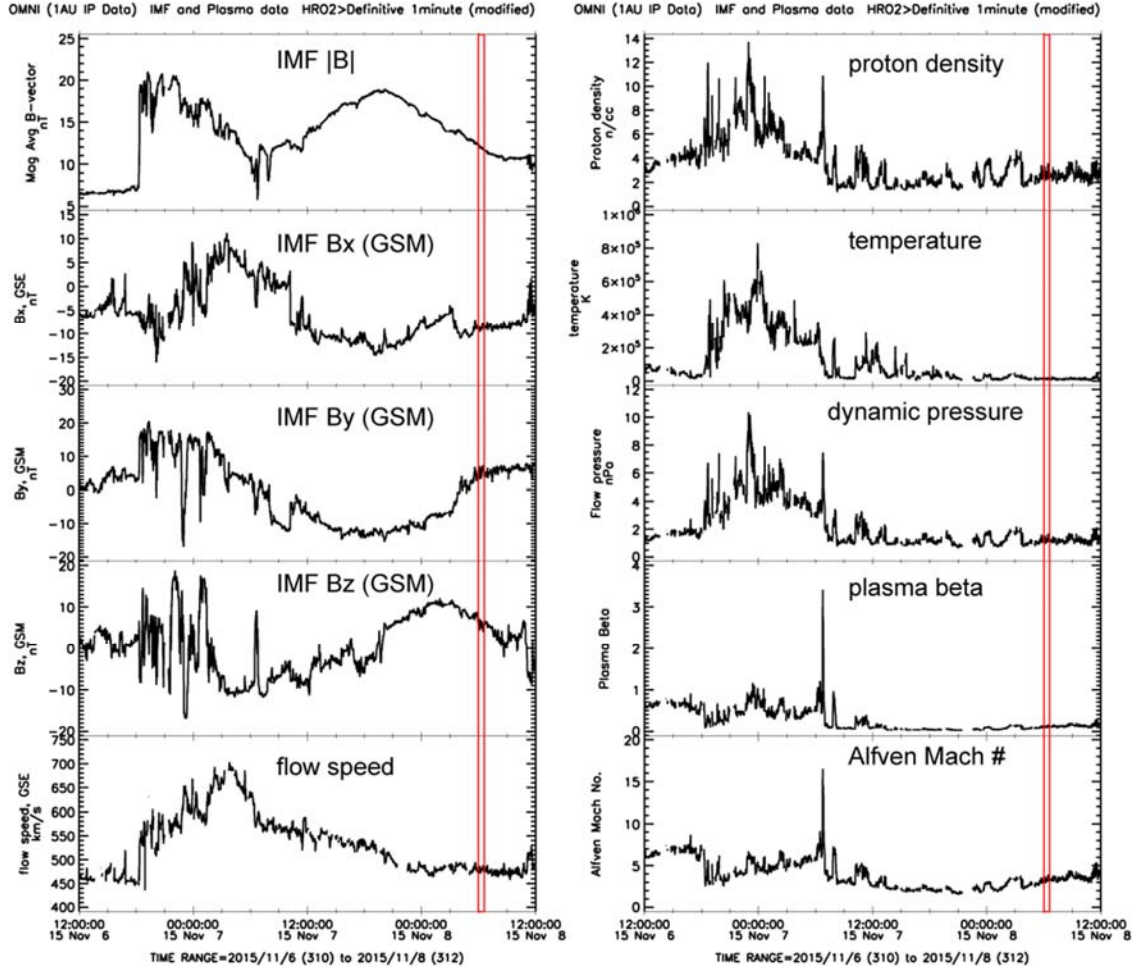


Figure S2. Solar wind and IMF conditions based on the OMNI database over a 2-day period from 2015-11-06, 1200 UT to 2015-11-08, 1200 UT, surrounding the MMS RX-only event on 2015-11-08. The red box marks the time interval studied in the main text.

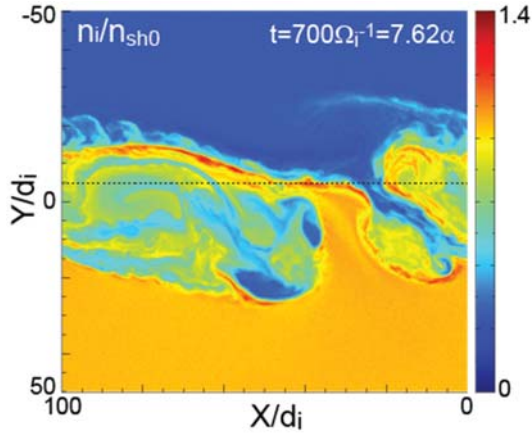


Figure S3. Density structure in a Kelvin-Helmholtz vortex from a three-dimensional (3D), fully kinetic simulation reported by Nakamura (2020). Simulated data taken from right to left along the virtual spacecraft path (dotted line) at $y = 4.8d_i$ are used as input for Bellan's method.

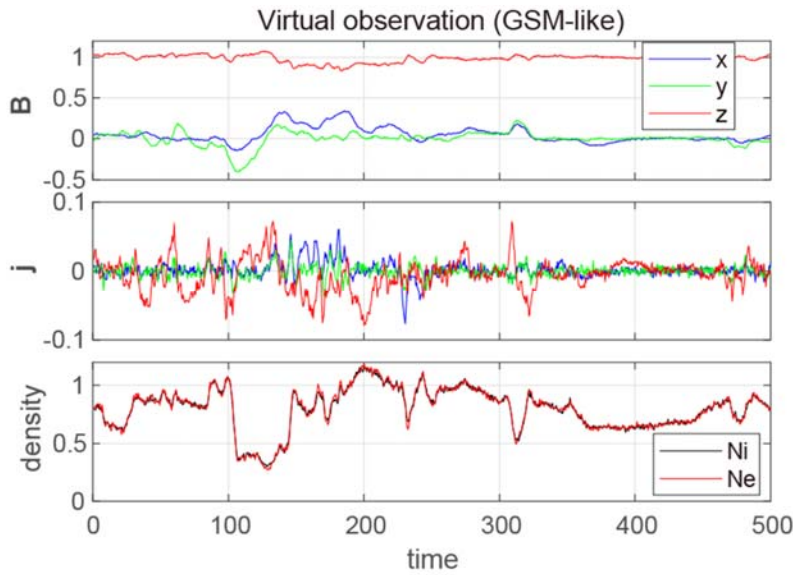


Figure S4. Virtual spacecraft measurements along the path shown in Figure S3, of which the magnetic field and current density are used as input for Bellan's method. The coordinate system is similar to that of GSM, with the x axis sunward and along the nominal magnetopause, the y axis duskward or normal to the magnetopause, and the z axis northward. See Nakamura, Hasegawa, et al. (2017) for details on the initial conditions and normalizations.

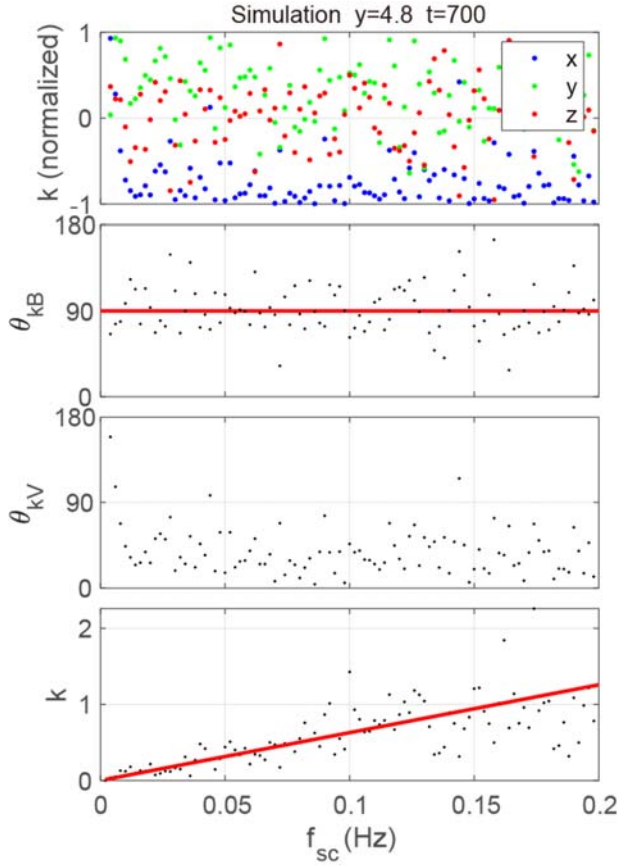


Figure S5. Properties of the k-vectors derived from Bellan's method (Bellan, 2016) applied to the virtual spacecraft data shown in Figure S4 in the same format as in Figure 5. The orientations of k-vectors and relationship between the magnitude of the wave number and spacecraft-frame frequency are very similar to those actually observed in the MMS KH instability event on 8 September 2015. Note that in the Nakamura, Hasegawa, et al. (2017) simulation, magnetic field fluctuations in KH vortices are of tangled 3D flux tubes resulting from vortex induced reconnection. Thus, the similarity of the magnetic power spectrum and k-vector properties between the simulation and MMS observation is consistent with our argument that the observed magnetic fluctuations are probably not of propagating waves but of tangled reconnected flux tubes advected by the background flow.

Table S1. Time intervals used to create the average magnetic spectra shown in Figure 3a.

Interval ID	Start time of the interval (UT)	End time of the interval (UT)
1	1007:10	1008:00
2	1008:30	1009:30
3	1009:40	1010:25
4	1010:40	1011:25
5	1011:35	1012:20
6	1012:45	1013:40

7	1014:00	1014:40
8	1015:00	1016:00
9	1016:10	1017:45
10	1018:00	1019:15
11	1020:10	1021:45
12	1022:15	1023:00
13	1023:20	1025:00
14	1025:35	1026:25
15	1026:40	1027:20
16	1027:40	1029:30
17	1029:45	1030:10
18	1030:40	1031:40
19	1032:05	1032:40
20	1033:00	1034:00
21	1034:45	1035:10
22	1035:35	1036:10
23	1036:40	1038:05
24	1039:35	1040:50
25	1041:10	1042:50
26	1043:20	1044:30
27	1045:00	1046:20
28	1046:40	1048:30
29	1049:00	1050:40
30	1051:30	1053:00
31	1053:30	1055:20
32	1055:40	1057:20
33	1058:00	1059:15
34	1059:40	1100:15
35	1100:37	1101:10
36	1102:20	1102:50
37	1103:10	1104:20
38	1105:15	1106:30
39	1107:00	1107:50
40	1108:10	1109:35
41	1109:55	1110:45
42	1111:05	1112:15
43	1112:35	1114:25
44	1114:55	1116:35
45	1117:15	1117:45
46	1118:05	1119:20
47	1120:00	1121:45
48	1121:50	1122:50
49	1123:15	1123:45
50	1124:25	1125:05
51	1126:05	1126:35

